Temporal variations of the mole fraction, carbon and hydrogen isotope ratios of atmospheric methane in the Hudson Bay Lowlands, Canada

Ryo Fujita[1*], Shinji Morimoto[1], Taku Umezawa[2], Kentaro Ishijima[3], Prabir K. Patra[3,1], Douglas E. J. Worthy[4], Daisuke Goto[5], Shuji Aoki[1], and Takakiyo Nakazawa[1]

[1]Center for Atmospheric and Oceanic Studies, Graduate School of Science, Tohoku University, Sendai, Japan
[2]National Institute for Environmental Studies, Tsukuba, Japan
[3]Japan Agency for Marine-Earth Science and Technology, Yokohama, Japan
[4]Environment and Climate Change Canada, Toronto, Ontario, Canada
[5]National Institute of Polar Research, Tokyo, Japan

Corresponding author: Ryo Fujita (ryo.fujita.t6@dc.tohoku.ac.jp)

Key Points:

- Mole fraction, $\delta^{13}C$, and δD of atmospheric CH_4 were measured at Churchill in the Hudson Bay Lowlands (HBL), Canada from 2007 to 2014
- CH_4, $\delta^{13}C$, and δD at Churchill are significantly affected by CH_4 emissions from surrounding wetlands, especially in summer
- Our best estimate of HBL CH_4 emissions is 2.7 ± 0.3 $TgCH_4$ yr^{-1}, which agrees well with those by recent inverse modeling studies

Keywords: methane, carbon and hydrogen isotopes, wetlands, Hudson Bay Lowlands

Abstract

We have conducted simultaneous measurements of the mole fraction and carbon and hydrogen isotope ratios ($\delta^{13}C$ and δD) of atmospheric methane (CH_4) at Churchill (58°44'N, 93°49'W) in the northern part of the Hudson Bay Lowlands (HBL), Canada since 2007. Compared with the measurements at an Arctic baseline monitoring station, Ny-Ålesund, Svalbard (78°55'N, 11°56'E), CH_4 mole fraction is generally higher and $\delta^{13}C$ and δD are lower at Churchill due to regional biogenic CH_4 emissions. Clear seasonal cycles in the CH_4 mole fraction, $\delta^{13}C$, and δD are observable at Churchill, and their seasonal phases in summer are earlier by approximately two weeks than those at Ny-Ålesund. Using the one-box model analysis, the phase difference is ascribed to the different seasonal influence of CH_4 emissions from boreal wetlands on the two sites. Short-term CH_4 variations are also observed at Churchill throughout the year. The analysis of the observed isotopic signatures of atmospheric CH_4 confirmed that the short-term CH_4 variations are mainly produced by biogenic CH_4 released from the HBL wetlands in summer and by fossil fuel CH_4 transported over the Arctic in winter. Forward simulations of an atmospheric chemistry-transport model, with wetland CH_4 fluxes prescribed by a process-based model, show unrealistically high CH_4 mole fractions at Churchill in summer, suggesting that CH_4 emissions assigned to the HBL wetlands are overestimated. Our best estimate of the HBL CH_4 emissions is 2.7 ± 0.3 $TgCH_4$ yr^{-1} as an average of 2007–2013, consistent with recent estimations by inverse modeling studies.

1 Introduction

Methane (CH_4) plays an important role in global climate change, as well as in atmospheric chemistry because CH_4 is the second most important anthropogenic long-lived greenhouse gas after CO_2 and its destruction occurs primarily by chemical reactions in the atmosphere. CH_4 is emitted from natural (wetlands, freshwater, wild animals, wildfires, termites, geological processes, ocean, hydrates, and permafrost) and anthropogenic (rice paddies, ruminants, landfills and waste, fossil fuels, and biomass burning) sources. CH_4 is mainly destroyed by reaction with OH radicals in the troposphere and partly by reactions with OH, Cl, and $O(^1D)$ in the stratosphere and by bacterial consumption in soils. Since the atmospheric CH_4 mole fraction shows large spatiotemporal variations due to unevenly distributed CH_4 sources/sinks and complicated atmospheric transport, an extensive and dense network of observations is required to depict a global picture of atmospheric CH_4 variations. For this purpose, observations of atmospheric CH_4 with grab sampling and continuous measurement techniques have been conducted mainly at ground-based stations since the 1970s (e.g., Aoki et al., 1992; Blake & Rowland, 1986; Cunnold et al., 2002; Dlugokencky et al., 2011; Rasmussenn & Khail, 1981). In the last few decades, the mole fraction of CH_4 showed unpredictable trends; the rate of increase in atmospheric CH_4 slowed down in the 1980s–1990s, leveled off from 1999 to 2006, and then rose again in 2006/2007 (Dlugokencky et al., 2009; Morimoto et al., 2017; Rigby et al., 2008). Such a CH_4 trend was examined in terms of ruminants, boreal and/or tropical wetlands, fossil fuels, or change in OH, but the cause is still controversial (e.g., Kirschke et al., 2013; Nisbet et al., 2016; Patra et al., 2016; Rigby et al., 2017; Schaefer et al., 2016; Turner et al., 2017). It is also known that there is a large discrepancy between CH_4 budgets estimated by top-down (inverse modeling using atmospheric measurements) and bottom-up (direct flux

measurement, statistical database, and process-based modeling) approaches, especially for natural sources (Kirschke et al., 2013; Saunois et al., 2016).

Systematic and high-precision observations of carbon and hydrogen isotope ratios ($\delta^{13}C$ and δD) of CH_4 provide us with additional constraints to understand the contribution of individual CH_4 sources to atmospheric CH_4 variations because each source has its own characteristic isotope ratio (e.g., Quay et al., 1999; Schwietzke et al., 2016; Sherwood et al., 2017; Whiticar & Schaefer, 2007). Their data would also help to close the gap in the CH_4 budget estimation between the top-down and bottom-up approaches through better source apportionment. $\delta^{13}C$ and δD are commonly defined by

$$\delta = \left(\frac{R_{sample}}{R_{standard}} - 1\right) \times 1000 \quad (‰). \tag{1}$$

Here, δ represents $\delta^{13}C$ or δD and R indicates $^{13}C/^{12}C$ or D/H. Subscripts '*sample*' and '*standard*' denote the sample and the standard, respectively, and as an international standard scale, VPDB is widely used for $\delta^{13}C$ and VSMOW for δD. Sherwood et al. (2017) recently reported by compiling a large number of isotope observation data that the biogenic, fossil fuel and biomass burning CH_4 sources have the respective mean isotope ratios of -61.7 ± 6.2 ($\pm$ 1 standard deviation (σ)), -44.8 ± 10.7, and -26.2 ± 4.8‰ for $\delta^{13}C$ and -317 ± 33, -197 ± 51, and -211 ± 15‰ for δD. Atmospheric background $\delta^{13}C$ and δD were also reported to be approximately −47 and −86‰, respectively (Allan et al., 2001; Whiticar & Schaefer, 2007). However, there have only been a few studies on simultaneous and high-precision measurements of atmospheric $\delta^{13}C$ and δD, which aim at examining atmospheric CH_4 variations (Rice et al., 2016; Röckmann et al., 2016; Tyler et al., 2007; Umezawa et al., 2012; Warwick et al., 2016).

The Hudson Bay Lowlands (HBL), the second largest continuous wetland in the world, is an important natural CH_4 source region in northern latitudes (Glooschenko et al., 1994). Nevertheless, there still remains a large uncertainty in magnitude, seasonality, and spatial distribution of CH_4 emissions in the HBL. Previous estimates of CH_4 emission rates for the HBL wetlands range from 0.2 to 11.3 $TgCH_4\ yr^{-1}$ (Melton et al., 2013; S. M. Miller et al., 2014, 2016; Pickett-Heaps et al., 2011; Roulet et al., 1994; Thompson et al., 2017; Worthy et al., 2000). In addition to the regional influence, the HBL area is also affected to some extent by anthropogenic CH_4 released in Europe and boreal Asia due to long-range air transport, especially in winter (Worthy et al., 1998, 2009). There may also be large anthropogenic CH_4 sources in Alberta located to the west of the HBL in association with natural gas production (S. M. Miller et al., 2014; Thompson et al., 2017). It is further pointed out that natural CH_4 sources such as ocean, geological seepages, subsea permafrost, and sea ice exist in the Arctic (e.g., Sapart et al., 2017; Walter et al., 2012). Therefore, to accurately estimate CH_4 emissions from the HBL wetlands based on the atmospheric CH_4 observations, it is necessary to examine the influence of anthropogenic and other natural CH_4 on its atmospheric variations.

To better understand the CH_4 cycle around the HBL, we started systematic air sampling at Churchill in 2007, situated in the northern part of the HBL, and analyzed those samples for the CH_4 mole fraction, $\delta^{13}C$, and δD. We present long-term, seasonal, and short-term variations of these three variables observed at the site and compare them with those at an Arctic baseline station, Ny-Ålesund, Svalbard (78°55'N, 11°56'E) (Morimoto et al., 2006, 2017). We then discuss the potential causes of temporal variations. By comparing the observed atmospheric CH_4

mole fractions with those simulated using an atmospheric chemistry transport model, we further examine CH_4 emissions in the HBL.

2 Method

2.1 Air sampling and analysis of CH_4 mole fraction, $\delta^{13}C$, and δD

Systematic observations of the CH_4 mole fraction and isotope ratios have been conducted at Churchill, Manitoba, Canada (58°44'N, 93°49'W) since April 2007, by a collaborative effort of the National Institute of Polar Research (NIPR), Tohoku University (TU) and Environment and Climate Change Canada (ECCC). The location of Churchill is shown in Figure 1, together with the land cover map of the HBL and its surrounding areas. Details of air sampling procedures and site description are found at the World Data Centre for Greenhouse Gases (WDCGG) website (https://ds.data.jma.go.jp/gmd/wdcgg/cgi-bin/wdcgg/accessdata.cgi?index=CHL458N00-EC&param=201208150002&select=parameter&parac=observation); thus, a brief explanation is presented here. Churchill is a small port city on the western shore of Hudson Bay with a population of about 900. The land cover around Churchill is mainly characterized by the Arctic tundra and the boreal forest. Air samples were taken from an intake mounted at the top of a 60-m high tower in the Churchill Northern Studies Centre (https://www.churchillscience.ca/), located 23 km east of the town of Churchill. Each air sample was automatically collected twice a week into a 2-L Pyrex glass flask at a pressure of 0.21 MPa, using a dedicated sampling system consisted of a separated line, a diaphragm pump, and a glass trap submerged in an –80°C methanol bath. The collected samples with a dew point of around –60°C were first analyzed at ECCC for mole fractions of various trace gases such as CO_2, CH_4, CO, N_2O, and SF_6, and then transported to NIPR, Japan at approximately 0.16–0.17 MPa for isotope analyses of atmospheric CH_4. At NIPR, each sample was divided into four 100-mL Pyrex glass flasks, two for the analysis of $\delta^{13}C$ at NIPR and two for δD at TU.

Observations at Ny-Ålesund, Svalbard (78°55'N, 11°56'E) to be compared with those at Churchill have been described by Morimoto et al. (2006) in detail. Air samples were collected once a week into 800-mL stainless steel flasks at 0.8 MPa and then sent to NIPR and TU for the mole fraction and isotope analyses.

Air samples collected at Churchill were analyzed for the CH_4 mole fraction at ECCC by using a gas chromatograph (Agilent 6890) equipped with a flame ionization detector (GC-FID) (Worthy et al., 1998) against the WMO-X2004A scale based on a gravimetric method (Dlugokencky et al., 2005, https://www.esrl.noaa.gov/gmd/ccl/ch4_scale.html). The repeatability of the CH_4 mole fraction analysis was estimated to be better than 2 ppb by analyzing the same sample repeatedly. CH_4 mole fractions of the air samples collected at Ny-Ålesund were determined using the GC-FID (Shimadzu, GC-8A) at NIPR relative to the TU1987 scale (Aoki et al., 1992; Morimoto et al., 2006). The results of the fifth and sixth WMO (World Meteorological Organization) Round-Robin intercomparison programs (https://www.esrl.noaa.gov/gmd/ccgg/wmorr/wmorr_results.php) showed that the TU2008 scale is higher than the WMO-X2004A scale by 2.5 ± 0.5 ppb on average. The TU2008 scale was also gravimetrically established by the same procedure as the TU1987, but a recently conducted close comparison of the two scales shows that the former provides lower CH_4 mole fractions by about

3.0 ppb than the latter at atmospheric CH_4 levels. Therefore, the difference between the TU1987 and WMO-X2004A scales is about 0.5 ppb. In this study, we compare the data at Churchill and Ny-Ålesund without any scale correction.

$\delta^{13}C$ of CH_4 was determined by using a gas chromatography-combustion isotope ratio mass spectrometer (GC-C-IRMS) based on MAT-252 (Thermo Fischer) with repeatability of 0.07‰ (Morimoto et al., 2006, 2009, 2017). The standard used in this analysis was pure CO_2 calibrated using a dual-inlet mass spectrometer against the TU $\delta^{13}C$ scale prepared from NBS-19 with $\delta^{13}C_{VPDB}$ of +1.95‰ (Nakazawa et al., 1993). In the daily $\delta^{13}C$ analysis, we analyzed a CH_4-in-air "test gas" with the known value of $\delta^{13}C$, stored in a 47-L aluminum cylinder, at least once a day to confirm the long-term stability of our $\delta^{13}C$ measurements. δD of CH_4 was obtained by using a gas chromatography-pyrolysis isotope ratio mass spectrometer (GC-P-IRMS) based on Delta Plus XP (Thermo Fischer) with repeatability of 2.2‰ (Umezawa et al., 2009). Our δD scale was established based on VSMOW (δD_{VSMOW} = 0‰) and SLAP (−428‰) using a dual-inlet mass spectrometer with a chromium reduction system at NIPR. To confirm the internal consistency of our δD analyses over a long period of time, we also analyzed a test gas at least twice on a measurement day and then corrected for potential day-to-day fluctuations of the measured δD arisen from changeable conditions of the GC-P-IRMS, assuming that the δD value of the test gas is stable with respect to time (Umezawa et al., 2009). The δD value of the test gas was determined using GC-P-IRMS against a reference gas (purified H_2) calibrated by VSMOW and SLAP.

The comparison of our $\delta^{13}C$ scale with that of the National Institute of Water and Atmospheric Research (NIWA) was carried out in 2004 and the result showed that our scale is 0.33 ± 0.04‰ higher than the NIWA scale (Morimoto et al., 2006, 2017). The comparison of our δD scale with that of the Institute for Marine and Atmospheric Research Utrecht carried out in 2013–2015 showed that our scale is lower by 13.1 ± 0.6‰ than theirs at ambient air levels (Umezawa et al., 2018). More information on the intercomparison of standard scales used in the CH_4 isotope community, including TU and NIPR, has been given in Umezawa et al. (2018).

2.2 Model simulation of CH_4 mole fraction

To interpret temporal variations of CH_4 in the atmosphere at Churchill and to estimate CH_4 emissions from the HBL, forward simulations of atmospheric CH_4 mole fraction were conducted for 2007–2013 using the CCSR/NIES/FRCGC (Center for Climate System Research /National Institute for Environmental Studies/Frontier Research Center for Global Change) AGCM-based Chemistry Transport Model (ACTM) developed at JAMSTEC (Japan Agency for Marine-Earth Science and Technology), with the setup described in Patra et al. (2016). ACTM uses a horizontal resolution of approximately 2.8° × 2.8° (T42 spectral truncation), with 67 pressure-sigma vertical layers. The atmospheric transport and tropospheric OH radical fields used in the model was validated by Patra et al. (2011, 2014).

Two CH_4 emission scenarios, "P16pri" and "P16pos", were used in this study, which are a priori and a posteriori CH_4 emissions of the global inverse modeling (Patra et al., 2016, corresponding to their "Case 2. CH4ags"). In the P16pri scenario, anthropogenic CH_4 emissions are adopted from EDGAR42FT (2013) and kept constant at the value of the year 2000, except for agricultural soils for which annual emissions are given until 2010 and then the value in 2010

is used repeatedly for 2011–2013. CH_4 emissions from biomass burning are taken from the combination of GISS (Goddard Institute for Space Studies) inventory (Fung et al., 1991) and GFED (Global Fire Emission Database) version 3.1 (van der Werf et al., 2010) after multiplying the GISS inventory by an optimal scaling factor (Patra et al., 2011). Biogenic (wetlands and rice paddies) CH_4 emissions are obtained from a process-based terrestrial ecosystem model, VISIT (Ito & Inatomi, 2012). The P16pos scenario is derived by optimizing the P16pri scenario using ACTM and CH_4 mole fraction observations (Patra et al., 2016). In forward simulations with ACTM and the above-mentioned two scenarios, atmospheric CH_4 is destroyed through reactions with OH, Cl, and $O^1(D)$, as well as through bacterial consumption in soils. Global OH field obtained by Spivakovsky et al. (2000) is scaled so that ACTM reproduces the observed decay rate of CH_3CCl_3 in the atmosphere (Patra et al., 2011, 2014). The soil sink is prepared by VISIT (Ito & Inatomi, 2012) and stratospheric loss by OH, Cl, and $O(^1D)$ is calculated using their concentration fields obtained by ACTM's stratospheric model run (Takigawa et al., 1999).

To investigate CH_4 source regions contributing to atmospheric CH_4 variations at Churchill, tagged tracer experiments were also performed using ACTM (Umezawa et al., 2014). In the experiments, the surface CH_4 emission field from the P16pos scenario was used. The global surface was first divided into 17 regions (Figure 2) and the forward simulation was performed for CH_4 released from each region. The region division is slightly different from that in Umezawa et al. (2014). In particular, we divided Boreal North America into four regions to better understand the regional contribution of CH_4 sources around Churchill. We defined the HBL area as 50°–60°N and 75°–96°W after Pickett-Heaps et al. (2011) (Region 14), the Province of Alberta as 50°–60°N and 110°–120°W after Thompson et al. (2017) (Region 12), and the border of western and eastern Canada as 96°W (Region 11 and Region 13).

3 Results and Discussion

3.1 Variations of CH_4 mole fraction, $\delta^{13}C$, and δD at Churchill and Ny-Ålesund

Figures 3 (a) – (c) show temporal variations of the CH_4 mole fraction, $\delta^{13}C$, and δD observed at Churchill and Ny-Ålesund for 2007–2014, together with best-fit curves to the data and long-term trends obtained using a digital-filtering technique (Nakazawa et al., 1997). In the filtering, an average seasonal cycle of each variable was approximated by fundamental and its first harmonics, and low-pass filters with cut-off periods of 4 and 24 months were adopted to obtain the best-fit curve and the long-term trend, respectively. As seen in Figure 3 (a), the CH_4 mole fraction at Churchill shows a clear seasonal cycle with a prominent minimum in June–July and a broad maximum in late winter, superimposed on an increasing trend. Similar characteristics are also observed at Ny-Ålesund. However, there are noticeable differences between the CH_4 variations at Churchill and Ny-Ålesund; (1) the annual mean CH_4 mole fraction is higher by 3–16 ppb at Churchill than at Ny-Ålesund for 2007–2013, (2) the timing of the seasonal CH_4 minimum is earlier by about one week, on average, at Churchill than at Ny-Ålesund (Figure 4 (a)), and (3) episodic high CH_4 mole fractions, sometimes over 2000 ppb, are frequently observed at Churchill throughout the year. A clear seasonal cycle is also observed in $\delta^{13}C$ and δD at Churchill and Ny-Ålesund, showing the maximum in early summer and the minimum in autumn. From inspection of the observation data at the two sites, it is obvious that (1) the annual means are lower by 0.1–0.2‰ for $\delta^{13}C$ and 1–4‰ for δD at Churchill than at Ny-Ålesund, (2) the average seasonal maxima of $\delta^{13}C$ and δD at Churchill precede those at Ny-

Ålesund by about two–three weeks (Figure 4 (b) – (c)), and (3) anomalously low $\delta^{13}C$ and δD values, below −48.5‰ for $\delta^{13}C$ and −115‰ for δD, are often observable at Churchill in the summertime. The differences in annual mean CH_4, $\delta^{13}C$ and δD between the two sites suggest that Churchill is more strongly affected by biogenic CH_4 sources with low $\delta^{13}C$ and δD than Ny-Ålesund. The seasonal phases of CH_4, $\delta^{13}C$, and δD at the two sites and the events with high CH_4 and low $\delta^{13}C$ and δD at Churchill are discussed in Section 3.2 and Section 3.3 in detail, respectively.

The seasonal cycles of CH_4 and $\delta^{13}C$ at Churchill and Ny-Ålesund are similar to those observed previously at other northern mid-to-high latitude sites (Dlugokencky et al., 2011; J. B. Miller et al., 2002; Nisbet et al., 2016; Tyler et al., 2007; Warwick et al., 2016). There are a few δD observations for the background atmosphere in northern mid-to-high latitudes (Tyler et al., 2007; Warwick et al., 2016). The seasonal cycles of δD observed by Warwick et al. (2016) at three northern high-latitude sites of Alert (82°N, 63°W), Barrow (71°N, 157°W), and Cold Bay (55°N, 163°W) are generally similar to those at Churchill and Ny-Ålesund.

The average growth rate of the CH_4 mole fraction at Churchill over 2007–2013 is 3.7 ± 0.5 ppb yr^{-1} (± 95% confidence interval (C.I.) derived using a residual bootstrap method (Davison & Hinkley, 1997)), which is slightly smaller than 4.9 ± 0.5 ppb yr^{-1} at Ny-Ålesund. The globally averaged CH_4 growth rate derived from the National Oceanic and Atmospheric Administration/ Earth System Research Laboratory (NOAA/ESRL) sites (http://www.esrl.noaa.gov/gmd/ccgg/trends_ch4/#global) for the same period is 5.3 ± 0.3 ppb yr^{-1} (1σ), which is comparable to the value at Ny-Ålesund. Dlugokencky et al. (2009) reported that the largest CH_4 increase of 13.7 ± 1.3 ppb yr^{-1} was observed at northern polar latitudes in 2007. A similar rapid CH_4 increase of 8.8 ± 3.0 ppb yr^{-1} was observed at Ny-Ålesund from 2007 to 2008, while no significant increase was detected at Churchill (1.1 ± 4.5 ppb yr^{-1}) for the same period (± 95% C.I.). As seen from Figure 3 (a), high CH_4 values were often observed in the warm season of 2007 at Churchill. If data collected in 2007 are excluded from the records of the two sites, the growth rate is 3.9 ± 0.7 ppb yr^{-1} for Churchill and 4.3 ± 0.6 ppb yr^{-1} for Ny-Ålesund, the values being close to each other.

No significant increasing or decreasing trend is found in $\delta^{13}C$ at Churchill for 2007–2013, with the rate of change of 0.005 ± 0.005‰ yr^{-1} (± 95% C.I.). In contrast to Churchill, a significant decrease of −0.007 ± 0.004‰ yr^{-1} was observed at Ny-Ålesund for the same period. The $\delta^{13}C$ trend at Churchill is probably due to the same reason as the low CH_4 growth rate, but with very low $\delta^{13}C$ values in the summer of 2007. By excluding the data for 2007, the rate of change in $\delta^{13}C$ is found to be −0.002 ± 0.006‰ yr^{-1}, which still shows no significant trends. Schaefer et al. (2016) and Nisbet et al. (2016) reported the secular decrease in $\delta^{13}C$ after 2006/2007, suggesting that biogenic CH_4 sources are predominantly responsible for the CH_4 increase after 2006. Long-term variations in CH_4 mole fraction and $\delta^{13}C$ at Ny-Ålesund in 1996–2013 have been discussed in Morimoto et al. (2017) in detail.

The average rates of increase in δD at Churchill and Ny-Ålesund for 2007–2013 are 0.43 ± 0.13 and 0.12 ± 0.10 ‰ yr^{-1}, respectively (± 95% C.I.). Since the δD data show relatively large inter-annual variability and its measurement uncertainty is larger than that of $\delta^{13}C$, it is difficult to robustly determine the trend; thus, we do not discuss the long-term variations in δD at this

stage. However, considering that δD is more sensitive to the chemical reaction of CH_4 with OH than $\delta^{13}C$ because of the larger kinetic isotope effect associated to the destruction of CH_3D in comparison with $^{12}CH_4$ and $^{13}CH_4$, further studies on atmospheric δD are required to improve our understanding of long-term changes and inter-annual variability in CH_4 sinks (e.g., McNorton et al., 2016; Monzka et al., 2011; Rigby et al., 2017; Turner et al., 2017).

3.2 Seasonal variations in CH_4 emissions

As mentioned above, the CH_4 mole fraction, $\delta^{13}C$, and δD vary seasonally at Churchill and Ny-Ålesund, and the seasonal minimum of CH_4 mole fraction and the seasonal maxima of $\delta^{13}C$ and δD at Churchill appear about two weeks earlier than those at Ny-Ålesund. To examine the contributions of biogenic, fossil fuel, and biomass burning CH_4 sources to the observed seasonal CH_4 cycle at Churchill and Ny-Ålesund, we employed a simple one-box model expressed by the following equations (Tyler et al., 2007; Umezawa, 2009);

$$\frac{dC_{ATM}}{dt} = S_{BIO} + S_{FF} + S_{BB} - kC_{ATM}\ , \tag{2}$$

$$\frac{d(C_{ATM}R_{C\_ATM})}{dt} = S_{BIO}R_{C\_BIO} + S_{FF}R_{C\_FF} + S_{BB}R_{C\_BB} - KIE^{C}kC_{ATM}R_{C\_ATM}\ , \tag{3}$$

$$\frac{d(C_{ATM}R_{D\_ATM})}{dt} = S_{BIO}R_{D\_BIO} + S_{FF}R_{D\_FF} + S_{BB}R_{D\_BB} - KIE^{D}kC_{ATM}R_{D\_ATM}\ , \tag{4}$$

where C_{ATM} is the observed value of the CH_4 mole fraction in the atmosphere; R_C and R_D denote the carbon and hydrogen isotope ratios (i.e., $^{13}C/^{12}C$ and D/H) of atmospheric (ATM), biogenic (BIO), fossil fuel (FF), and biomass burning (BB) CH_4, respectively; *S* indicates the seasonally variable contributions of the three CH_4 sources; and *k* is the pseudo-first order rate coefficient for OH + CH_4. In this analysis, the observed atmospheric monthly values of C_{ATM}, R_{C_ATM}, and R_{D_ATM} are derived by adding the average seasonal cycle to the average annual value for 2007–2013 (Figure 4). The respective isotopic signatures of BIO, FF, and BB sources (R_C and R_D) were assumed to be −61.7 ± 6.2 (± 1σ), −44.8 ± 10.7, and −26.2 ± 4.8‰ for $\delta^{13}C$ and −317 ± 33, −197 ± 51, and −211 ± 15‰ for δD (Sherwood et al., 2017). *k* was calculated based on the TransCom CH_4 settings (Patra et al., 2011), equivalent to the atmospheric lifetime of 10.3 yr. KIE^C and KIE^D are the overall kinetic isotope effects (KIE) for the carbon and hydrogen isotopes in the CH_4 destruction processes. In this model, KIE^C and KIE^D were set to 1.0067 and 1.275, respectively, by averaging the KIE values for the CH_4 destruction by OH in the troposphere, OH, $O(^1D)$, and Cl in the stratosphere, and absorption by soils after weighting the respective isotope effects with relevant CH_4 destruction fluxes (see Table S2 in Rice et al., (2016)). The uncertainty ranges (± 1σ) of KIE^C and KIE^D were assumed to correspond to ± 20% of the isotope fractionation factor ε (ε = 1/KIE – 1), i.e., ε^C = −6.7 ± 1.3‰ and ε^D = −216 ± 43‰. The present uncertainty range of ε^C is almost consistent with the estimate by Schaefer et al. (2016). The parameters used in this box model analysis are summarized in Table S1 in Supporting Information. For uncertainty estimation of this model analysis, we assumed that the respective source isotopic signatures and *KIE*s distribute normally around their mean values with 1σ, and then ran the Monte Carlo simulation 5000 times by randomly sampling the normally distributed

isotopic signatures, *KIE*s, and average seasonal cycles of CH_4, $\delta^{13}C$, and δD (Figure 4). By using the 5000 pseudo datasets thus generated, we calculated the median and 68 percentile confidence intervals of the monthly contributions of the respective CH_4 sources (*S*s).

Figures 5 (a) and (b) show the calculated monthly contributions of individual CH_4 sources (S_{BIO}, S_{FF}, S_{BB}) for Churchill and Ny-Ålesund, respectively, together with those of CH_4 destruction by OH. As seen in Figure 5, biogenic sources of CH_4 are the most dominant ones for the seasonal cycle of atmospheric CH_4 observed at Churchill and Ny-Ålesund, with large contributions in summer. This source would be boreal wetlands, since there is a vast amount of wetlands (e.g., bogs, fens, and tundra) in northern high latitudes from which a large quantity of CH_4 is released, showing a strong seasonal variation unlike anthropogenic biogenic CH_4 (e.g., ruminants, landfills, and waste) (Melton et al., 2013 and references therein). The biogenic CH_4 contribution at Churchill begins in May, reaches a maximum in July, and then ceases in November (Figure 5 (a)). This seasonality is probably associated with soil temperature rise and snow melting, the highest soil temperature, and low surface temperatures and snow cover in the respective months (e.g., Pickett-Heaps et al. 2011).

Previous measurements of CH_4 fluxes indicate that the CH_4 emissions from boreal wetlands peak in June–August (e.g., Whalen & Reeburgh, 1992). However, there are large differences in the strength and seasonality of their measured CH_4 fluxes, mainly due to large spatial and temporal variability of CH_4 emissions. Pickett-Heaps et al. (2011) estimated the CH_4 emissions from the HBL using the GEOS-Chem chemical transport model and the atmospheric CH_4 mole fraction data at Fraserdale and Alert, Canada and found that the seasonal maximum occurs in July. S. M. Miller et al. (2014) also suggested from their regional inversion that CH_4 emissions from the HBL reach a maximum in July. The Bayesian atmospheric inversion model results by Thompson et al. (2017) showed that the CH_4 flux in the HBL increases gradually in spring, reaches a maximum in August–September, and declines rapidly in September–October.

Seasonal variations of the contribution of biogenic CH_4 estimated for Churchill and Ny-Ålesund are slightly different from each other (Figures 5 (a) and (b)). For example, the biogenic CH_4 is discernible at Churchill in May, but there is no appearance of such a contribution at Ny-Ålesund. Moreover, the seasonal maximum of the biogenic CH_4 contribution appears in July at Churchill and in August at Ny-Ålesund. This difference is presumably attributable to the influence of local/regional wetland CH_4 emissions on Churchill, as well as to different latitudes of the two sites. Churchill is located on the northern perimeter of the HBL; thus, CH_4 emitted from HBL wetlands could directly affect the CH_4 mole fraction at Churchill. On the other hand, since Ny-Ålesund is far from strong CH_4 sources, seasonal signals of CH_4 emissions from boreal wetlands may reach the site with a time lag. It is also noteworthy that the onset of wetland CH_4 emissions is earlier at lower latitudes due to the latitude-dependent seasonal temperature pattern.

It is also found in Figure 5 that fossil fuel and biomass burning are minor contributors to the seasonal CH_4 cycle. However, more detailed inspection of the results indicates that fossil fuel sources significantly influence the atmospheric CH_4 mole fraction both at Churchill and Ny-Ålesund in early winter. Fossil fuel sources of CH_4 emissions are usually regarded as non-seasonal sources (EDGAR42FT, 2013), but the contribution of fossil fuel CH_4 emissions could be enhanced in winter, especially in northern high-latitude regions. For example, natural gas is consumed in large quantities during the cold season, during which the transport pipelines are pressurized so that a significant leakage of CH_4 may occur (Lowry et al., 2001). In addition to fossil fuel CH_4 emissions, slow vertical air mixing due to the strong inversion layer and weak

destruction of CH_4 with OH may strengthen the influence of the fossil fuel CH_4 source on the wintertime increase of atmospheric CH_4.

Biomass burning is also known to have seasonality in CH_4 emission, mainly due to seasonally varying rainfall and temperature. GFED3 shows that the maximum CH_4 emissions from biomass burning occur in July in northern high latitudes (> 50°N) (van der Werf et al., 2010). However, in this study, only small seasonal variations are detected for CH_4 emissions from biomass burning. Although the summertime maximum of biomass burning CH_4 emissions is detected both at Churchill and Ny-Ålesund, the values are not statistically significant.

We also see at Churchill and Ny-Ålesund that the chemical destruction by OH varies seasonally as large as biogenic CH_4. Since CH_4 is a long-lived species whose atmospheric lifetime is longer than one year even in summer, OH in remote areas would play an important role in the observed CH_4 variations both at two sites. Therefore, we used OH concentration and temperature data averaged over 30°–90°N and 700–1000 hPa in the present one-box model analysis. Other CH_4 sinks, such as soil oxidation and stratospheric loss, also contribute to the CH_4 seasonal cycle to some extent. The results of the one-box model analysis are further affected by values adopted for the isotopic signatures of CH_4 sources and *KIE*s. To inspect the sensitivity of our model analysis results to these variables, we made the one-box model analysis again using the parameters different from the initial set (see Table S1). The results of the sensitivity tests obtained for the two sites, shown in Figure S1 to Figure S3, indicate that the seasonal contributions obtained under various conditions are generally consistent to that derived with our initially set parameters.

3.3 Short-term variations of CH_4 mole fraction, $\delta^{13}C$ and δD

The CH_4 mole fraction sometimes shows extremely high values at Churchill throughout the year. Similar anomalous data are also found in $\delta^{13}C$ and δD with extremely low values, although such data are observed only in the summertime. In this study, 596, 605, and 600 data are available for the CH_4 mole fraction, $\delta^{13}C$, and δD, respectively. By defining the data deviated from the best-fit curve by more than 3σ of the fit as outliers, 50, 41, and 19 data were selected out from the respective records of the CH_4 mole fraction, $\delta^{13}C$, and δD.

To investigate the cause of the 50 outliers with extremely high CH_4 mole fractions in terms of emission sources, the "Miller/Tans plot" represented by

$$C_{obs}\delta_{obs} - C_{BGD}\delta_{BGD} = (C_{obs} - C_{BGD})\delta_S \quad (5)$$

was applied to the CH_4 mole fraction, $\delta^{13}C$, and δD data (J. B. Miller & Tans, 2003; Umezawa et al., 2012). Here, C and δ represent the CH_4 mole fraction and corresponding $\delta^{13}C$ (or δD), respectively, and subscripts *obs*, *BGD*, and *S* denote the observed, background, and source values, respectively. The mean isotope ratio of the source, δ_S, can be obtained as a slope of the regression line of $C_{obs}\delta_{obs} - C_{BGD}\delta_{BGD}$ and $C_{obs} - C_{BGD}$. In this analysis, the background value for each variable is given by the best-fit curve of the related observation data.

Figures 6 (a) and (b) show the Miller/Tans plots for $\delta^{13}C$ and δD, respectively. It is found from the figures that the summertime (May–October) and wintertime (November–April) slopes are significantly different from each other. By applying an ordinary least squares regression to

each cluster, the summertime data yield the slopes of −63.3 ± 2.8‰ (± 95% C.I; correlation coefficient R = −0.96) for $\delta^{13}C$ and −327 ± 26‰ (R = −0.92) for δD, while the wintertime data provide the corresponding values of −47.7 ± 4.3‰ (R = −0.96) and −241 ± 48‰ (R = −0.89). The summertime slopes agree well with those expected from biogenic CH_4 sources (e.g., Sherwood et al., 2017; Whiticar & Schaefer, 2007), suggesting the influence of CH_4 emissions from the HBL wetlands. On the other hand, the wintertime slopes result in much heavier isotope ratios than the summertime slopes, the values being close to the isotopic signatures of fossil fuel CH_4.

Previous studies reported that the $\delta^{13}C$ and δD values of CH_4 released from wetlands in northern high latitudes range from −60 to −80‰ and from −300 to −420‰, respectively (e.g., Nakagawa et al., 2002; Walter et al., 2008). Our summertime $\delta^{13}C$ and δD slope values fall in previously reported ranges for the respective variables. Measurements taken by Kuhlmann et al. (1998) for two days at Fraserdale, Ontario in August 1995 show that the isotopic signature of CH_4 from regional wetlands is −60.0 ± 3.2‰ for $\delta^{13}C$ and −442 ± 142‰ for δD. These values are consistent with our summertime values within estimated uncertainty limits, although their δD estimate is more negative than ours on average.

Worthy et al. (1998, 2009) show that the air is often transported from Siberia and Europe to the Canadian high Arctic region in winter, by which Canada is widely covered with polluted air masses originated in the Eurasian Continent. To investigate the highly elevated CH_4 mole fractions observed at Churchill in winter, a seven-day backward trajectory analysis was conducted using the HYSPLIT model (Stein et al., 2015). In this analysis, each air parcel was released from 500 m above sea level over Churchill at the time when the high CH_4 mole fraction was observed. The results show that the air parcels wander around Churchill in summer, while the wintertime air parcels go back to more distant areas, mainly northern high latitudes (Figure 7). The backward trajectory analysis also shows that some air parcels assigned to high CH_4 mole fractions observed at Churchill in winter are originated from Western Canada (Figure 7 (b)). In this connection, S. M. Miller et al. (2014) and Thompson et al. (2017) reported recently that a large amount of CH_4 is presumably released from Alberta, Western Canada in association with natural gas production.

There are also other minor natural CH_4 sources, such as ocean, geological seepages, subsea permafrost, and sea ice, in the Arctic region, of which isotopic signatures are close to the values of wetlands and/or fossil fuel sources (e.g., Sapart et al., 2017; Walter et al., 2012). As mentioned above, the backward trajectory analysis indicates that Churchill is strongly influenced by air masses from the HBL and its surroundings in summer. This suggests that the summertime CH_4 enhancement at Churchill is mainly due to wetlands rather than these minor sources. On the other hand, it is difficult to distinguish anthropogenic fossil fuel origin from natural geologic origin in winter using the backward trajectory analysis. However, some wintertime high CH_4 events at Churchill were found to be coincident with high CO and CO_2 mole fractions, suggesting the influence of human activities.

3.4 Model simulation of atmospheric CH_4 variations

To investigate CH_4 emissions from the HBL in more detail, we simulated the atmospheric CH_4 mole fraction at Churchill by using ACTM and two CH_4 emission scenarios, P16pri and P16pos. The atmospheric CH_4 mole fractions simulated for 2007–2013 are shown in Figure 8 (a),

451 together with the observed values. For comparison, the results for Ny-Ålesund are also shown in
452 Figure 8 (b). As seen in the figures, CH_4 mole fractions simulated for Ny-Ålesund reproduce
453 general features of the observed CH_4 variations, while obvious discrepancies between the
454 simulated and observed mole fractions are seen at Churchill. The CH_4 mole fractions simulated
455 using both scenarios for Churchill frequently overestimate and underestimate the summertime
456 and wintertime values, respectively. It is also found at the two sites that the model-simulated
457 CH_4 mole fractions based on P16pri are higher than the observations for 2007–2010 as a whole.
458 In this connection, Patra et al. (2016) mentioned that a priori emissions used in their inversion
459 (i.e., P16pri scenario) are too high early in the 2000s. On the other hand, P16pos reproduces
460 fairly well the long-term trends of atmospheric CH_4 at the two sites.

461 To see the degree of model-observation agreement at each site, the correlation coefficient
462 (R) and the root-mean-square error (RMSE) of the simulated and observed CH_4 mole fractions
463 for each scenario are summarized in Table 1. These statistical parameters were calculated from
464 the respective curves fitted to the simulated and observed data (Nakazawa et al., 1997). R
465 generally indicates the degree of agreement between the model calculation and observation for
466 the seasonal phase of atmospheric CH_4, since the seasonal CH_4 cycle is larger in amplitude than
467 inter-annual variations. RMSE is a measure of how well the model reproduces the observed CH_4
468 variations.

469 The respective correlation coefficients obtained for the P16pri and P16pos scenarios are
470 0.22 and 0.36 for Churchill and 0.57 and 0.95 for Ny-Ålesund (Table 1). The results of Ny-
471 Ålesund show that the observed seasonality of atmospheric CH_4 is reproduced fairly well by the
472 model for either scenario and that the agreement between the model and observation is much
473 improved by employing P16pos rather than P16pri. RMSE is also decreased by replacing P16pri
474 with P16pos, suggesting an improvement of the model-observation agreement. On the other
475 hand, the two statistics, R and RMSE, for Churchill indicate that there is no appreciable
476 improvement even if the scenario is altered. It should be noted that the P16pos scenario was
477 derived from the inversion calculation by including the CH_4 mole fraction data observed at
478 Zeppelin Station, Ny-Ålesund, but with no observation data around the HBL (Patra et al., 2016).
479 Therefore, the model with P16pos shows a much better agreement with observed CH_4 variations
480 at Ny-Ålesund rather than at Churchill.

481 To improve the agreement between the model-simulated and observed seasonal CH_4
482 cycles at Churchill, we first examined the cause for this discrepancy. The average seasonal CH_4
483 cycle at Churchill and Ny-Ålesund, derived by applying the digital filtering technique to the
484 observed and model-calculated CH_4 mole fractions, is plotted in Figure 9 after adding the
485 average CH_4 mole fraction over 2007–2013 at the respective sites. Since the OH fields and the
486 atmospheric transport of ACTM are validated (Patra et al., 2011, 2014), the difference between
487 the observed and model-generated seasonal CH_4 cycles could be mainly attributable to CH_4
488 emissions adopted in model simulations.

489 Figure 9 (c) shows the difference between the average seasonal CH_4 cycles at Churchill
490 and Ny-Ålesund (defined as ΔCH_4) for each scenario or the observation. Since the variations at
491 Ny-Ålesund are representative of northern high latitudes, ΔCH_4 would be closely related to CH_4
492 emissions around Churchill. The observations yield the maximum ΔCH_4 of approximately 15
493 ppb in late July and December–January. On the other hand, model simulations show the
494 maximum ΔCH_4 of up to 40–60 ppb in late July, which is three to four times the observational
495 result. This suggests that both P16pri and P16pos scenarios overestimate the summertime CH_4

emissions around Churchill. As shown in Figure 5, we found at Churchill and Ny-Ålesund that CH_4 emissions from biogenic and fossil fuel sources dominate the CH_4 mole fractions in summer and winter, respectively, and biomass burning is not important for the seasonality of atmospheric CH_4. Therefore, the summertime and wintertime maxima of ΔCH_4 are likely associated with the respective emissions of CH_4 from wetlands and fossil fuels around Churchill.

Since the model-observation disagreement is remarkably larger in summer than in winter, we focus our discussion on the summertime events. To clarify which regions contribute to the summertime overestimated CH_4 mole fractions, we conducted tagged tracer experiments as described in Section 2.2. The calculated contributions of the respective regions to the average seasonal CH_4 cycles at Churchill and Ny-Ålesund are shown in Figure 10. Also shown in the figure are the observed and model-simulated (P16pos) average seasonal CH_4 cycles.

It is obvious from Figure 10 that the HBL (rg14), Western Canada/Alaska (rg11), and Europe (rg02) have a large influence on the seasonal CH_4 cycle at Churchill. However, the model-generated seasonal CH_4 cycles for the HBL and Western Canada/Alaska are quite different from the observed results, particularly in seasonal phase. CH_4 originated in these regions are emitted mostly from boreal wetlands. Therefore, the reproduction of the observed seasonal CH_4 cycle by the model can be greatly improved by reducing the summertime CH_4 emissions, especially from the HBL. In this regard, the forward simulations with the P16pos scenario can reproduce relatively well the CH_4 mole fractions at Alert (82°N, 63°W), Barrow (71°N, 157°W), Cold Bay (55°N, 163°W), and Estevan Point (49°N, 127°W) (Patra et al., 2016), which suggests that the CH_4 emissions around the four background sites (Western Canada/Alaska) are constrained fairly well.

3.5 CH_4 emissions from the HBL wetlands

Assuming that the seasonal CH_4 cycle at Churchill is strongly affected by nearby CH_4 sources in the warm months, we made a rough estimation of CH_4 emissions from the HBL. In this estimation, (1) the seasonality of CH_4 emissions from the HBL for May–October was set so as to follow the seasonal variations in biogenic CH_4 sources derived by the one-box model analysis, and (2) the annual CH_4 emission strength of the HBL was adjusted to minimize the RMSE between the modeled and observed seasonal CH_4 cycles at Churchill over 2007–2013, based on the forward simulation of ACTM with the emission scenario modified above ("P16pos_rev" in Table 1 and Figure 9). To keep the global CH_4 emissions unchanged, the same amount of CH_4 as the reduced summertime emission for the HBL was added to the Province of Alberta (Region 12) as non-seasonal CH_4 emissions. This method is based on the results of the previous studies that the anthropogenic CH_4 emissions in Alberta could be underestimated in EDGAR4.2FT (S. M. Miller et al., 2014; Thompson et al., 2017). As mentioned above, the model simulations with P16pos made for Churchill underestimate the observed CH_4 mole fractions in winter. Additional CH_4 emissions in Alberta would contribute to improving this discrepancy.

The best agreement between the observed and model-simulated CH_4 variations is obtained by reducing the HBL CH_4 emissions for May–October to 30%, as an average for 2007–2013, of their original values given by the P16pos. This reduction corresponds to a fall to 39% of the original annual emission given by the P16pos scenario (6.9 ± 0.4 $TgCH_4$ yr^{-1}). The result yields 2.7 ± 0.3 $TgCH_4$ yr^{-1} as the average HBL CH_4 emission for 2007–2013. Note that this

emission value includes CH_4 released not only from wetlands but also from other sources such as human activities and biomass burning. However, total CH_4 emissions from sources other than wetlands could be very small (~ 0.2 $TgCH_4\ yr^{-1}$), since the a priori P16pri indicates that wetland CH_4 emissions account for 94% of the total in the HBL. With respect to the reduction in CH_4 emissions for May–October in our results, the resultant percent value could be an upper limit in the estimation of CH_4 emissions from the HBL, since the summertime CH_4 mole fractions observed at Churchill are affected not only by the HBL but also by the other regions to some extent.

There still remain large differences in CH_4 emissions estimated for the HBL region. For example, the ABLE-3B/NOWES airborne and ground observation campaign, conducted in the summer of 1990, estimated annual CH_4 emissions as 0.5 ± 0.3 $TgCH_4\ yr^{-1}$ for the HBL (Roulet et al., 1994). The inverse approach based on the atmospheric CH_4 observations at Fraserdale and Alert estimated the annual CH_4 emissions as 0.2–0.5 $TgCH_4\ yr^{-1}$ (Worthy et al., 2000), similar to the result obtained by Roulet et al. (1994). On the other hand, Pickett-Heaps et al. (2011) calculated CH_4 emissions from the HBL as 2.3 $TgCH_4\ yr^{-1}$ using a chemical transport model and surface observations of atmospheric CH_4. A process model intercomparison project (The Wetland and Wetland CH_4 Intercomparison of Models Project; WETCHIMP) showed CH_4 emissions from the HBL at the range of 2.2–11.3 $TgCH_4\ yr^{-1}$ (Melton et al., 2013). Wetland CH_4 emissions calculated by VISIT, used as a priori flux to derive the P16pos scenario, yield 5.7 ± 0.5 $TgCH_4\ yr^{-1}$ for the HBL region, which lies near the middle of the nine results from WETCHIMP. Recently, two inversion studies based on atmospheric CH_4 data reported the HBL CH_4 emissions as 2.4 ± 0.3 $TgCH_4\ yr^{-1}$ (S. M. Miller et al., 2014) and 2.7–3.4 $TgCH_4\ yr^{-1}$ (Thompson et al., 2017), which are lower than the results of most process model studies, but close to the estimate by Pickett-Heaps et al. (2011). Our estimate of 2.7 ± 0.3 $TgCH_4\ yr^{-1}$ is also comparable to the results of these top-down studies, as well as to the lower values of WETCHIMP.

As mentioned above, CH_4 emissions reduced in the HBL were transferred to the Province of Alberta. By this additional amount of CH_4, the annual emissions of 2.6 ± 0.3 $TgCH_4\ yr^{-1}$ allocated by P16pos to Alberta is now increased to 6.9 ± 0.5 $TgCH_4\ yr^{-1}$ in the P16pos_rev scenario. Thompson et al. (2017) estimated the CH_4 flux in Alberta to be 5.0–5.8 $TgCH_4\ yr^{-1}$ based on their Bayesian inversion, which is smaller than our estimate by 1.1–1.9 $TgCH_4\ yr^{-1}$. By adopting P16pos_rev instead of P16pos, we found that the CH_4 mole fractions observed at two continental tower sites operated by ECCC, Lac La Biche (55°N, 113°W) and East Trout Lake (54°N, 105°W) (http://ds.data.jma.go.jp/gmd/wdcgg/wdcgg.html) (see Figure 1(a)), are better reproduced by the ACTM forward simulation; the two towers are located in and near the Alberta region, defined as 50°–60°N and 110°–120°W in this study. It is also seen in Figure 9 (a) that not only the summertime minimum but also the wintertime maximum of the average seasonal CH_4 cycle at Churchill is simulated well by P16pos_rev rather than by P16pos. Consequently, our analyses support the results of S. M. Miller et al. (2014) and Thompson et al. (2017) that EDGAR42FT underestimates the anthropogenic CH_4 emissions in the Province of Alberta.

4 Summary and conclusions

We measured the mole fraction, $\delta^{13}C$, and δD of atmospheric CH_4 at Churchill (58°44'N, 93°49'W) on the northern perimeter of the Hudson Bay Lowlands (HBL), Canada from a grab

584 sampling method for 2007–2014. Compared to the measurements at Ny-Ålesund, Svalbard
585 (78°55'N, 11°56'E), which is away from regional CH_4 sources, the CH_4 mole fraction is
586 generally higher and $\delta^{13}C$ and δD are lower at Churchill, suggesting CH_4 emissions from
587 regional/local boreal wetlands around the site.

588 The seasonal cycle of CH_4 ($\delta^{13}C$) is clearly observable, with the maximum value in
589 January–February (May) and the minimum in June (October). δD also shows high values in June
590 and low values in cold months of September to March. The summer minimum (maximum) of the
591 CH_4 mole fraction ($\delta^{13}C$ and δD) appears approximately two weeks earlier at Churchill than at
592 Ny-Ålesund. The simple mass balance analysis with the one-box model indicates that the
593 seasonal maximum of biogenic CH_4 influence at Churchill precedes the maximum at Ny-
594 Ålesund, contributing to the phase difference of atmospheric CH_4, $\delta^{13}C$, and δD between the two
595 sites.

596 Short-term variations in the CH_4 mole fraction are observed throughout the year at
597 Churchill, with higher values especially in the summertime. By inspecting the relationship
598 between the short-term variations of the CH_4 mole fraction and isotope ratios, $\delta^{13}C$ and δD of
599 related CH_4 sources are estimated to be respectively -63.3 ± 2.8 and -327 ± 26‰ for the
600 summertime (May–October), and -47.7 ± 4.3 and -241 ± 48‰ for the wintertime (November–
601 April). These values indicate that short-term CH_4 variations observed at Churchill are produced
602 mainly by biogenic CH_4 emissions from wetland in summer and fossil fuel sources in winter.

603 To investigate the seasonal cycle of atmospheric CH_4 in terms of CH_4 sources, we
604 simulated the atmospheric CH_4 mole fractions using ACTM with two CH_4 emission scenarios,
605 and then compared them with the observed results at Churchill and Ny-Ålesund. ACTM
606 overestimates the CH_4 mole fraction at Churchill in summer, although the seasonal CH_4 cycle at
607 Ny-Ålesund is reproduced well. Tagged tracer experiments indicate that the summertime high
608 CH_4 mole fractions at Churchill are mainly caused by the air transported from the HBL. This
609 implies that the wetland CH_4 fluxes prescribed for the region in the ACTM simulations are
610 overestimated. By adjusting the CH_4 fluxes prescribed for the HBL in ACTM so that the
611 seasonal CH_4 cycle observed at Churchill is reproduced well, average CH_4 emission from the
612 HBL for 2007–2013 is estimated to be 2.7 ± 0.3 $TgCH_4$ yr^{-1}, which is in good agreement with
613 the results of previous modeling studies based on atmospheric CH_4 observations.

614 This study shows that simultaneous and high precision measurements of the mole
615 fraction, $\delta^{13}C$, and δD provide us with valuable information on CH_4 sources. It is also shown
616 from the model-observation comparison that systematic observations of the atmospheric CH_4
617 mole fraction in nearby source regions are important for assessing the local/regional CH_4
618 emissions. Inclusion of $\delta^{13}C$ and δD into the model analysis would provide additional strong
619 constraints on a better understanding of CH_4 sources and sinks. For this purpose, further efforts
620 are needed not only to increase systematic observations of $\delta^{13}C$ and δD, but also to undertake an
621 extensive intercomparison program of $\delta^{13}C$ and δD scales among related institutes.

622

623 **Acknowledgments**

624 We express our sincere thanks to LeeAnn Fishback, scientific coordinator at the
625 Churchill Northern Studies Centre for her efforts to air sample collection and Michele Ernst at

ECCC for her logistical coordination of the flask program and air sample analyses. We are also grateful to Hiroko Nagamoto, NIPR and Morimasa Sato, TU for their support to isotope analyses. This work was partly supported by NIPR through the Project Research Nos. KP-15 and KP-304, the Arctic Challenge for Sustainability (ArCS) project by the Ministry of Education, Culture, Sports, Science and Technology, Japan, and the JSPS KAKENHI Grant Nos. 23310012 and 15H03722. The $\delta^{13}C$ and δD data are available from the website at TU (http://caos.sakura.ne.jp/tgr/data/en/). The CH_4 mole fraction data at Churchill, Lac La Biche and East Trout Lake are available from the WDCGG website (http://ds.data.jma.go.jp/gmd/wdcgg/wdcgg.html).

References

Allan, W., Manning M. R., Lassey, K. R., Lowe, D. C., & Gomez, A. J. (2001). Modeling the variation of $\delta^{13}C$ in atmospheric methane: Phase ellipses and the kinetic isotope effect. *Global Biogeochemical Cycles*, *15*(2), 467–481. https://doi.org/10.1029/2000GB001282

Aoki, S., Nakazawa, T., Murayama, S., & Kawaguchi, S. (1992). Measurements of atmospheric methane at the Japanese Antarctic Station, Syowa. *Tellus B*, *44*(4), 273–281. https://doi.org/10.3402/tellusb.v44i4.15455

Arino, O., Perez, R., Julio, J., Kalogirou, V., Bontemps, S., Defourny, P., & Van Bogaert, E. (2012). Global land cover map for 2009 (GlobCover 2009). European Space Agency (ESA) & Université catholique de Louvain (UCL). [Available at http://www.esa-landcover-cci.org]

Blake, D. R., & Rowland, F. S. (1986). World-wide increase in tropospheric methane, 1978–1983. *Journal of Atmospheric Chemistry*, *4*(1), 43–62. https://doi.org/10.1007/BF00053772

Cunnold, D. M., Steele, L. P., Fraser, P. J., Simmonds, P. G., Prinn, R. G., Weiss, R. F., et al. (2002). In situ measurements of atmospheric methane at GAGE/AGAGE sites during 1985–2000 and resulting source inferences. *Journal of Geophysical Research: Atmospheres*, *107*(D14), 4225. https://doi.org/10.1029/2001JD001226

Davison, A. C., & Hinkley, V. (1997), Bootstrap methods and their application. *Cambridge Series in Statistical and Probabilistic Mathematics*, Cambridge Univ. Press, New York.

Dlugokencky, E. J., Bruhwiler, L., White, J. W. C., Emmons, L. K., Novelli, P. C., Montzka, S. A., et al. (2009). Observational constraints on recent increases in the atmospheric CH_4 burden. *Geophysical Research Letters*, *36*, L18803. https://doi.org/10.1029/2009GL039780

Dlugokencky, E. J., Myers, R. C., Lang, P. M., Masarie, K. A., Crotwell, A. M., Thoning, K. W., et al. (2005). Conversion of NOAA atmospheric dry air CH_4 mole fractions to a gravimetrically prepared standard scale. *Journal of Geophysical Research: Atmosphere*, *110*, D18306. https://doi.org/10.1029/2005JD006035

Dlugokencky, E. J., Nisbet, E. G., Fisher, R., & Lowry, D. (2011). Global atmospheric methane: budget, changes and dangers. *Philosophical Transactions of the Royal Society a: Mathematical, Physical and Engineering Sciences*, *369*, 2058–2072. https://doi.org/10.1098/rsta.2010.0341

EDGAR42FT (2013). Global emissions EDGAR v4.2 FT2010. [Available at http://edgar.jrc.ec.europa.eu/overview.php?v=42FT2010]

Fisher, R. E., France, J. L., Lowry, D., Lanoisellé, M., Brownlow, R., Pyle, J. A., et al. (2017). Measurement of the ^{13}C isotopic signature of methane emissions from northern European wetlands. *Global Biogeochemical Cycles*, *31*(3), 605–623. https://doi.org/10.1002/2016GB005504

Fung, I., John, J., Lerner, J., Matthews, E., Prather, M., Steele, L. P., & Fraser, P. J. (1991). Three-dimensional model synthesis of the global methane cycle. *Journal of Geophysical Research: Atmospheres*, *96*(D7), 13033–13065. https://doi.org/10.1029/91JD01247

Glooschenko, W. A., Roulet, N. T., Barrie, L. A., Schiff, H. I., & McAdie, H. G. (1994). The Northern Wetlands Study (NOWES): An overview. *Journal of Geophysical Research: Atmospheres*, *99*(D1), 1423–1428. https://doi.org/10.1029/93JD02184

Ito, A., & Inatomi, M. (2012). Use of a process-based model for assessing the methane budgets of global terrestrial ecosystems and evaluation of uncertainty. *Biogeosciences*, *9*(2), 759–773. https://doi.org/10.5194/bg-9-759-2012

Kirschke, S., Bousquet, P., Ciais, P., Saunois, M., Canadell, J. G., Dlugokencky, E. J., et al. (2013). Three decades of global methane sources and sinks. *Nature Geoscience*, *6*, 813–823. https://doi.org/10.1038/ngeo1955

Kuhlmann, A. J., Worthy, D. E. J., Trivett, N. B. A., & Levin, I. (1998). Methane emissions from a wetland region within the Hudson Bay Lowland: An atmospheric approach. *Journal of Geophysical Research: Atmospheres*, *103*(D13), 16009–16016. https://doi.org/10.1029/98JD01024

Lowry, D., Holmes, C. W., Rata, N. D., O'Brien, P., & Nisbet, E. G. (2001). London methane emissions: Use of diurnal changes in concentration and $\delta^{13}C$ to identify urban sources and verify inventories. *Journal of Geophysical Research: Atmospheres*, *106*(D7), 7427–7448. https://doi.org/10.1029/2000JD900601

McNorton, J., Chipperfield, M. P., Gloor, M., Wilson, C., Feng, W., Hayman, G. D., et al. (2016). Role of OH variability in the stalling of the global atmospheric CH_4 growth rate from 1999 to 2006. *Atmospheric Chemistry and Physics*, *16*(12), 7943–7956. https://doi.org/10.5194/acp-16-7943-2016

Melton, J. R., Wania, R., Hodson, E. L., Poulter, B., Ringeval, B., Spahni, R., et al. (2013). Present state of global wetland extent and wetland methane modelling: conclusions from a model inter-comparison project (WETCHIMP). *Biogeosciences*, *10*(2), 753–788. https://doi.org/10.5194/bg-10-753-2013

Miller, J. B., Mack, K. A., Dissly, R. D., Dlugockenky, E. J., & Tans, P. P. (2002). Development of analytical methods and measurements of $^{13}C/^{12}C$ in atmospheric CH_4 from the NOAA Climate Monitoring and Diagnostics Laboratory Global Air Sampling Network. *Journal of Geophysical Research: Atmospheres*, *107*(D13), 4178. https://doi.org/10.1029/2001JD000630

Miller, J. B., & Tans, P. P. (2003). Calculating isotopic fractionation from atmospheric measurements at various scales. *Tellus B*, *55*(2), 207–214. https://doi.org/10.1034/j.1600-0889.2003.00020.x

Miller, S. M., Commane, R., Melton, J. R., Andrews, A. E., Benmergui, J., Dlugokencky, E. J., et al. (2016). Evaluation of wetland methane emissions across North America using atmospheric data and inverse modeling. *Biogeosciences*, *13*(4), 1329–1339. https://doi.org/10.5194/bg-13-1329-2016

Miller, S. M., Worthy, D. E. J., Michalak, A. M., Wofsy, S. C., Kort, E. A., Havice, T. C., et al. (2014). Observational constraints on the distribution, seasonality, and environmental predictors of North American boreal methane emissions. *Global Biogeochemical Cycles*, *28*, 146–160. https://doi.org/doi:10.1002/2013GB004580

Montzka, S. A., Krol, M., Dlugokencky, E., Hall, B., Jöckel, P., & Lelieveld, J. (2011). Small interannual variability of global atmospheric hydroxyl. *Science*, *331*(6013), 67–69. https://doi.org/10.1126/science.1197640

Morimoto, S., S. Aoki, and T. Nakazawa (2009). High precision measurements of carbon isotopic ratio of atmospheric methane using a continuous flow mass spectrometer, Antarctic Record, 53(1), 1–8.

Morimoto, S., Aoki, S., Nakazawa, T., & Yamanouchi, T. (2006). Temporal variations of the carbon isotopic ratio of atmospheric methane observed at Ny-Ålesund, Svalbard from 1996 to 2004. *Geophysical Research Letters*, *33*, L01807. https://doi.org/10.1029/2005GL024648

Morimoto, S., Fujita, R., Aoki, S., Goto, D., & Nakazawa, T. (2017). Long-term variations of the mole fraction and carbon isotope ratio of atmospheric methane observed at Ny-Ålesund, Svalbard from 1996 to 2013. *Tellus B 69*(1), 1380497. https://doi.org/10.1080/16000889.2017.1380497

Nakagawa, F., Yoshida, N., Nojiri, Y., & Makarov, V. (2002). Production of methane from alasses in eastern Siberia: Implications from its ^{14}C and stable isotopic compositions. *Global Biogeochemical Cycles*, *16*(3). https://doi.org/10.1029/2000GB001384

Nakazawa, T., Ishizawa, M., Higuchi, K., & Trivett, N. B. A. (1997). Two curve fitting methods applied to CO_2 flask data. *Environmetrics*, *8*(3), 197–218. https://doi.org/10.1002/(SICI)1099-095X(199705)8:3<197::AID-ENV248>3.0.CO;2-C

Nakazawa, T., S. Morimoto, S. Aoki, and M. Tanaka (1993). Time and space variations of the carbon isotopic ratio of tropospheric carbon dioxide over Japan. *Tellus B, 45*(3), 258–274. https://doi.org/10.1034/j.1600-0889.1993.t01-2-00004.x

Nisbet, E. G., Dlugokencky, E. J., Manning, M. R., Lowry, D., Fisher, R. E., France, J. L., et al. (2016). Rising atmospheric methane: 2007–2014 growth and isotopic shift. *Global Biogeochemical Cycles*, *30*(9), 1356–1370. https://doi.org/10.1002/2016GB005406

Patra, P. K., Houweling, S., Krol, M., Bousquet, P., Belikov, D., Bergmann, D., et al. (2011). TransCom model simulations of CH_4 and related species: linking transport, surface flux and chemical loss with CH_4 variability in the troposphere and lower stratosphere. *Atmospheric Chemistry and Physics*, *11*(24), 12813–12837. https://doi.org/10.5194/acp-11-12813-2011

Patra, P. K., Krol, M. C., Montzka, S. A., Arnold, T., Atlas, E. L., Lintner, B. R., et al. (2014). Observational evidence for interhemispheric hydroxyl-radical parity. *Nature*, *513*, 219–223. https://doi.org/10.1038/nature13721

Patra, P. K., Saeki, T., Dlugokencky, E. J., Ishijima, K., Umezawa, T., Ito, A., et al. (2016). Regional methane emission estimation based on observed atmospheric concentrations (2002–2012). *Journal of the Meteorological Society of Japan*, *94*(1), 91–113. https://doi.org/10.2151/jmsj.2016-006

Pickett-Heaps, C. A., Jacob, D. J., Wecht, K. J., Kort, E. A., Wofsy, S. C., Diskin, G. S., et al. (2011). Magnitude and seasonality of wetland methane emissions from the Hudson Bay Lowlands (Canada). *Atmospheric Chemistry and Physics*, *11*(8), 3773–3779. https://doi.org/10.5194/acp-11-3773-2011

Quay, P., Stutsman, J., Wilbur, D., Snover, A., Dlugokencky, E., & Brown, T. (1999). The isotopic composition of atmospheric methane. *Global Biogeochemical Cycles*, *13*(2), 445–461. https://doi.org/10.1029/1998GB900006

Rasmussen, R. A., & Khalil, M. A. K. (1981). Atmospheric methane (CH_4): Trends and seasonal cycles. *Journal of Geophysical Research: Atmospheres*, *86*(C10), 9826–9832. https://doi.org/10.1029/JC086iC10p09826

Rice, A. L., Butenhoff, C. L., Teama, D. G., Röger, F. H., Khalil, M. A. K., & Rasmussen, R. A. (2016). Atmospheric methane isotopic record favors fossil sources flat in 1980s and 1990s with recent increase. *Proceedings of the National Academy of Sciences*, *113*(39), 10791–10796. https://doi.org/10.1073/pnas.1522923113

Rigby, M., Montzka, S. A., Prinn, R. G., White, J. W. C., Young, D., O'Doherty, S., et al. (2017). Role of atmospheric oxidation in recent methane growth. *Proceedings of the National Academy of Sciences*, *114*(21), 5373–5377. https://doi.org/10.1073/pnas.1616426114

Rigby, M., Prinn, R. G., Fraser, P. J., Simmonds, P. G., Langenfelds, R. L., Huang, J., et al. (2008). Renewed growth of atmospheric methane. *Geophysical Research Letters*, *35*, L22805. https://doi.org/10.1029/2008GL036037

Roulet, N. T., Jano, A., Kelly, C. A., Klinger, L. F., Moore, T. R., Protz, R., et al. (1994). Role of the Hudson Bay lowland as a source of atmospheric methane. *Journal of Geophysical Research: Atmospheres*, *99*(D1), 1439–1454. https://doi.org/10.1029/93JD00261

Röckmann, T., Eyer, S., van der Veen, C., Popa, M. E., Tuzson, B., Monteil, G., et al. (2016). In situ observations of the isotopic composition of methane at the Cabauw tall tower site. *Atmospheric Chemistry and Physics*, *16*(16), 10469–10487. https://doi.org/10.5194/acp-16-10469-2016

Sapart, C. J., Shakhova, N., Semiletov, I., Jansen, J., Szidat, S., Kosmach, D., et al. (2017). The origin of methane in the East Siberian Arctic Shelf unraveled with triple isotope analysis. *Biogeosciences*, *14*(9), 2283–2292. https://doi.org/10.5194/bg-14-2283-2017

Saueressig, G., Crowley, J. N., Bergamaschi, P., Brühl, C., Brenninkmeijer, C. A. M., & Fischer, H. (2001). Carbon 13 and D kinetic isotope effects in the reactions of CH_4 with $O(^1D)$ and OH: New laboratory measurements and their implications for the isotopic composition of stratospheric methane. *Journal of Geophysical Research: Atmospheres*, *106*(D19), 23127–23138. https://doi.org/10.1029/2000JD000120

Saunois, M., Bousquet, P., Poulter, B., Peregon, A., Ciais, P., Canadell, J. G., et al. (2016). The global methane budget 2000–2012. *Earth System Science Data*, *8*(2), 697–751. https://doi.org/10.5194/essd-8-697-2016

Schaefer, H., Fletcher, S. E. M., Veidt, C., Lassey, K. R., Brailsford, G. W., Bromley, T. M., et al. (2016). A 21st-century shift from fossil-fuel to biogenic methane emissions indicated by $^{13}CH_4$. *Science*, *352*(6281), 80–84. https://doi.org/10.1126/science.aad2705

Schwietzke S., Sherwood, O. A., Bruhwiler, L. M. P., Miller, J. B., Etiope, G., Dlugokencky, E. J., et al. (2016). Upward revision of global fossil fuel methane emissions based on isotope database, *Nature*, *538*, 88–91. https://doi.org/10.1038/nature19797

Sherwood, O. A., Schwietzke, S., Arling, V. A., & Etiope, G. (2017). Global inventory of gas geochemistry data from fossil fuel, microbial and burning sources, version 2017. *Earth System Science Data*, *9*(2), 639–656. https://doi.org/10.5194/essd-9-639-2017

Spivakovsky, C. M., Logan, J. A., Montzka, S. A., Balkanski, Y. J., Foreman-Fowler, M., Jones, D. B. A., et al. (2000). Three-dimensional climatological distribution of tropospheric OH: Update and evaluation. *Journal of Geophysical Research: Atmospheres*, *105*(D7), 8931–8980. https://doi.org/10.1029/1999JD901006

Stein, A. F., Draxler, R. R., Rolph, G. D., Stunder, B. J. B., Cohen, M. D., & Ngan, F. (2015). NOAA's HYSPLIT atmospheric transport and dispersion modeling system. *Bulletin of the American Meteorological Society*, *96*, 2059–2077. https://doi.org/10.1175/BAMS-D-14-00110.1

Takigawa, M., Takahashi, M., & Akiyoshi, H. (1999). Simulation of ozone and other chemical species using a Center for Climate System Research/National Institute for Environmental Studies atmospheric GCM with coupled stratospheric chemistry. *Journal of Geophysical Research: Atmospheres*, *104*(D11), 14003–14018. https://doi.org/10.1029/1998JD100105

Thompson, R. L., Sasakawa, M., Machida, T., Aalto, T., Worthy, D., Lavric, J. V., et al. (2017). Methane fluxes in the high northern latitudes for 2005–2013 estimated using a Bayesian atmospheric inversion. *Atmospheric Chemistry and Physics*, *17*(5), 3553–3572. https://doi.org/10.5194/acp-17-3553-2017

Turner, A. J., Frankenberg, C., Wennberg, P. O., & Jacob, D. J. (2017). Ambiguity in the causes for decadal trends in atmospheric methane and hydroxyl. *Proceedings of the National Academy of Sciences*, *114*(21), 5367–5372. https://doi.org/10.1073/pnas.1616020114

Tyler, S. C., Rice, A. L., & Ajie, H. O. (2007). Stable isotope ratios in atmospheric CH_4: Implications for seasonal sources and sinks. *Journal of Geophysical Research: Atmospheres*, *112*, D03303. https://doi.org/10.1029/2006JD007231

Umezawa, T. (2009). A study of global methane cycle based on measurements of its carbon and hydrogen isotopes in the atmosphere, (Doctoral dissertation). Tohoku University, Japan.

Umezawa, T., Aoki, S., Nakazawa, T., & Morimoto, S. (2009). A high-precision measurement system for carbon and hydrogen isotopic ratios of atmospheric methane and its application to air samples collected in the western Pacific region. *Journal of the Meteorological Society of Japan*, *87*(3), 365–379. https://doi.org/10.2151/jmsj.87.365

Umezawa, T., Brenninkmeijer, C. A. M., Röckmann, T., van der Veen, C., Tyler, S. C., Fujita, R., et al. (2018). Interlaboratory comparison of $\delta^{13}C$ and δD measurements of atmospheric CH_4 for combined use of data sets from different laboratories. *Atmospheric Measurement Techniques*, *11*, 1207–1231. https://doi.org/10.5194/amt-11-1207-2018

Umezawa, T., Goto, D., Aoki, S., Ishijima, K., Patra, P. K., Sugawara, S., et al. (2014). Variations of tropospheric methane over Japan during 1988–2010. *Tellus B*, *66*(1), 23837. https://doi.org/10.3402/tellusb.v66.23837

Umezawa, T., Machida, T., Aoki, S., & Nakazawa, T. (2012). Contributions of natural and anthropogenic sources to atmospheric methane variations over western Siberia estimated from its carbon and hydrogen isotopes. *Global Biogeochemical Cycles*, *26*, GB4009. http://doi.org/10.1029/2011GB004232

van der Werf, G. R., Randerson, J. T., Giglio, L., Collatz, G. J., Mu, M., Kasibhatla, P. S., et al. (2010). Global fire emissions and the contribution of deforestation, savanna, forest, agricultural, and peat fires (1997–2009). *Atmospheric Chemistry and Physics*, *10*(23), 11707–11735. https://doi.org/10.5194/acp-10-11707-2010

Walter Anthony, K. M., Anthony, P., Grosse, G., & Chanton, J. (2012). Geologic methane seeps along boundaries of Arctic permafrost thaw and melting glaciers. *Nature Geoscience*, *5*(6), 419–426. https://doi.org/10.1038/NGEO1480

Walter, K. M., Chanton, J. P., Chapin, F. S., III, Schuur, E. A. G., & Zimov, S. A. (2008). Methane production and bubble emissions from arctic lakes: Isotopic implications for source pathways and ages. *Journal of Geophysical Research: Biogeosciences*, *113*, G00A08. https://doi.org/10.1029/2007JG000569

Warwick, N. J., Cain, M. L., Fisher, R., France, J. L., Lowry, D., Michel, S. E., et al. (2016). Using $\delta^{13}C$-CH_4 and δD-CH_4 to constrain Arctic methane emissions. *Atmospheric Chemistry and Physics*, *16*(23), 14891–14908. https://doi.org/10.5194/acp-16-14891-2016

Whalen, S. C., & Reeburgh, W. S. (1992). Interannual variations in tundra methane emission: A 4-year time series at fixed sites. *Global Biogeochemical Cycles*, *6*(2), 139–159. https://doi.org/10.1029/92GB00430

Whiticar, M., & Schaefer, H. (2007). Constraining past global tropospheric methane budgets with carbon and hydrogen isotope ratios in ice. *Philosophical Transactions of the Royal Society a: Mathematical, Physical and Engineering Sciences*, *365*, 1793–1828. https://doi.org/10.1098/rsta.2007.2048

Worthy, D. E. J., Chan, E., Ishizawa, M., Chan, D., Poss, C., Dlugokencky, E. J., et al. (2009). Decreasing anthropogenic methane emissions in Europe and Siberia inferred from continuous carbon dioxide and methane observations at Alert, Canada. *Journal of Geophysical Research: Atmospheres*, *114*, D10301. https://doi.org/10.1029/2008JD011239

Worthy, D. E. J., Levin, I., Hopper, F., Ernst, M. K., & Trivett, N. B. A. (2000). Evidence for a link between climate and northern wetland methane emissions. *Journal of Geophysical Research: Atmospheres*, *105*(D3), 4031–4038. https://doi.org/10.1029/1999JD901100

Worthy, D. E. J., Levin, I., Trivett, N. B. A., Kuhlmann, A. J., Hopper, J. T., & Ernst, M. K. (1998). Seven years of continuous methane observations at a remote boreal site in Ontario, Canada. *Journal of Geophysical Research: Atmospheres*, *103*(D13), 15995–16007. https://doi.org/10.1029/98JD00925

838 **Figure 1**. (a) Map showing the locations of Churchill, Canada (58°44'N, 93°49'W; site code:
839 CHL) (red circle), Ny-Ålesund (78°55'N, 11°56'E; NAL) (blue circle), Alert (82°N, 63°W;
840 ALT), Barrow (71°N, 157°W; BRW), Cold Bay (55°N, 163°W; CBA), Estevan Point (49°N,
841 127°W; ESP), Lac La Biche (55°N, 113°W; LLB), and East Trout Lake (54°N, 105°W; ETL)
842 (black squares), and (b) surface coverage around the Hudson Bay Lowlands (Arino et al., 2012).
843
844 **Figure 2**. A map showing 17 source regions (boxes) and their CH_4 emissions (colors) for the
845 tagged tracer experiments on the atmospheric CH_4 mole fractions at Churchill and Ny-Ålesund.
846 The colors represent annual averages over 2007–2013 based on the P16pos scenario. Red circle,
847 blue circle, and black squares have the same meaning as in Figure 1 (a).
848
849 **Figure 3.** Measured values of (a) the mole fraction, (b) $\delta^{13}C$ and (c) δD of atmospheric CH_4 at
850 Churchill (red circles) and Ny-Ålesund (blue circles). Also shown are the best-fit curves to the
851 observed data (thin lines) and long-term trends (thick lines), derived using the digital-filtering
852 technique. The observation data are classified into two groups, one is baseline data lying within 3
853 times the standard deviation (σ) of the residual of the best-fit curve (closed circles) and one is
854 outliers that deviate by more than 3σ from the best-fit curve (open circles). The outliers are
855 excluded to derive the best-fit curves.
856
857 **Figure 4.** Average seasonal cycles of (a) the CH_4 mole fraction, (b) $\delta^{13}C$ and (c) δD observed at
858 Churchill (red lines) and Ny-Ålesund (blue lines) for 2007–2013. Dotted lines represent the 95
859 percentile bootstrap confidence intervals (see text). Each average seasonal cycle is plotted after
860 adding its average value for 2007–2013.
861
862 **Figure 5.** Monthly contributions of biogenic (BIO), fossil fuel (FF) and biomass burning (BB)
863 CH_4 sources to the seasonal CH_4 cycle estimated using the one-box model for (a) Churchill and
864 (b) Ny-Ålesund. Error bars denote the 68 percentile confidence intervals derived by the Monte
865 Carlo method with 5000 pseudo time series. Open circles connected with line are the monthly
866 values of CH_4 destruction by OH.
867
868 **Figure 6.** Miller/Tans plots of (a) $\delta^{13}C$ and (b) δD versus the CH_4 mole fraction for Churchill in
869 summer (May–October, blue circles) and winter (November–April, red squares). Solid and
870 dotted lines represent linear regression lines and 95% confidence intervals, respectively.
871
872 **Figure 7.** 7-day backward trajectories with one hour interval (dots) for high CH_4 mole fractions
873 observed at Churchill (red circle) in (a) May–October and (b) November–April. Shaded bar
874 represents the altitude of air parcel released. For each event, nine air parcels were simultaneously
875 released from 500 m above sea level, one over Churchill and the other eight over 30 km south,
876 north, west and east of Churchill, and 42 km southwest, southeast, northwest and northeast of
877 Churchill. Red circle, blue circle, and black squares have the same meaning as in Figure 1 (a).
878
879 **Figure 8.** Comparison of the observed (black dots) and model-calculated CH_4 mole fractions
880 (colors) at (a) Churchill and (b) Ny-Ålesund for 2007–2013. Light blue and red dots represent
881 the values calculated using ACTM with the respective scenarios of P16pri and P16pos.
882

883 **Figure 9.** Average seasonal cycles of the observed (black lines) and model-simulated (color
884 lines) CH_4 mole fraction at (a) Churchill and (b) Ny-Ålesund, and (c) seasonal differences of the
885 CH_4 mole fraction between Churchill and Ny-Ålesund. Each average seasonal cycle is plotted
886 after adding the average mole fraction for 2007–2013.
887
888 **Figure 10.** Comparison of the observed average seasonal CH_4 cycles (black solid lines) with the
889 contributions of the respective regions (cf. Figure 2) estimated by tagged tracer experiments
890 (color lines) at (a) Churchill and (b) Ny-Ålesund. Purple, yellow, green and red lines represent
891 the contributions from Region 2 (Europe), Region 5 (Western Siberia), Region 11 (Western
892 Canada/Alaska) and Region 14 (Hudson Bay Lowland), respectively. The other regions with
893 minor contributions are shown in gray. Black dotted line in each panel is the average seasonal
894 CH_4 cycle calculated using ACTM with the P16pos scenario, which is equivalent to the sum of
895 contributions from Region 1–17.
896
897 **Table 1.** Summary of the statistics (R and RMSE) calculated for the comparison of the CH_4 mole
898 fractions simulated by ACTM with three CH_4 emission scenarios (P16pri, P16pos and
899 P16pos_rev) with the observed values at Churchill (CHL) and Ny-Ålesund (NAL).
900

	P16pri		**P16pos**		**P16pos_rev**	
Statistics	**CHL**	**NAL**	**CHL**	**NAL**	**CHL**	**NAL**
R	0.22	0.57	0.36	0.95	0.91	0.94
RMSE	25.8	17.9	16.2	8.7	6.6	9.3

901

Figure 1.

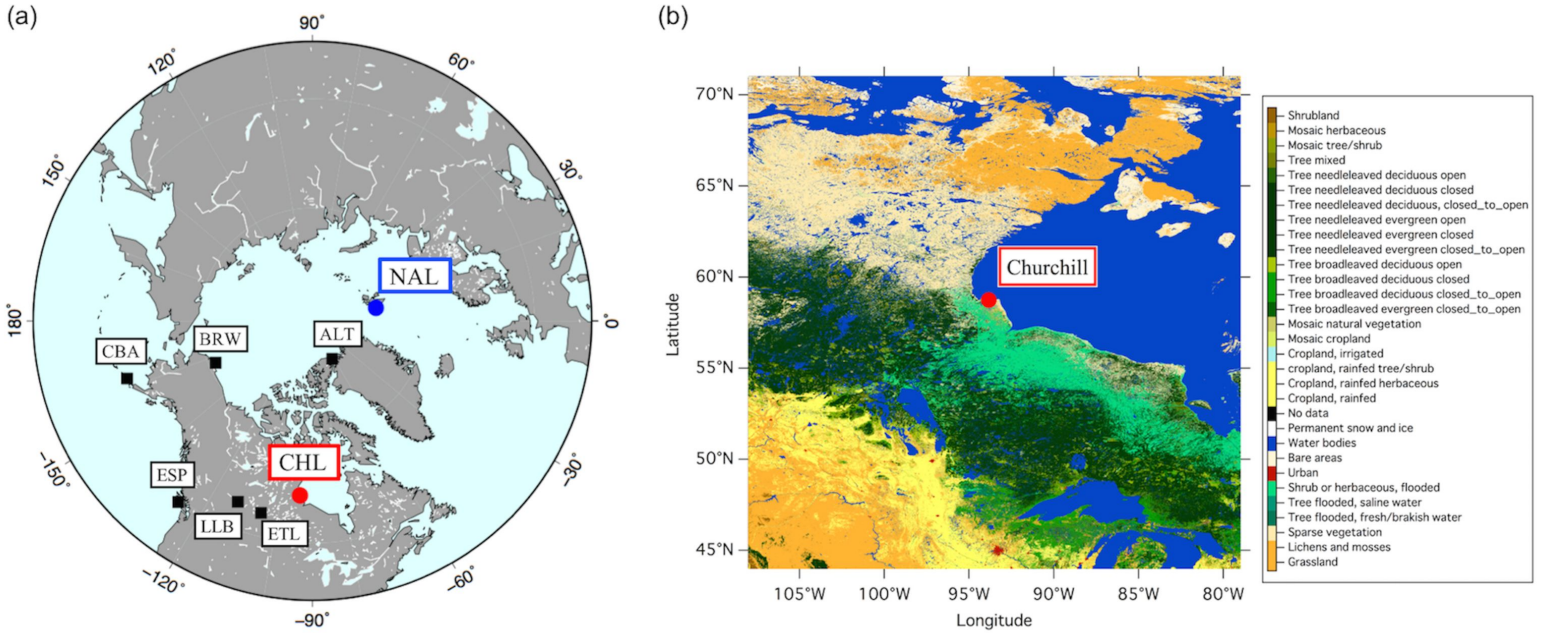
(a)
90°
120°
60°
150°
30°
180°
0°
−150°
−30°
−120°
−60°
−90°
NAL
BRW
ALT
CBA
CHL
ESP
LLB
ETL
(b)
70°N
65°N
60°N
55°N
50°N
45°N
Latitude
105°W
100°W
95°W
90°W
85°W
80°W
Longitude
Churchill
Shrubland
Mosaic herbaceous
Mosaic tree/shrub
Tree mixed
Tree needleleaved deciduous open
Tree needleleaved deciduous closed
Tree needleleaved deciduous, closed_to_open
Tree needleleaved evergreen open
Tree needleleaved evergreen closed
Tree needleleaved evergreen closed_to_open
Tree broadleaved deciduous open
Tree broadleaved deciduous closed
Tree broadleaved deciduous closed_to_open
Tree broadleaved evergreen closed_to_open
Mosaic natural vegetation
Mosaic cropland
Cropland, irrigated
cropland, rainfed tree/shrub
Cropland, rainfed herbaceous
Cropland, rainfed
No data
Permanent snow and ice
Water bodies
Bare areas
Urban
Shrub or herbaceous, flooded
Tree flooded, saline water
Tree flooded, fresh/brakish water
Sparse vegetation
Lichens and mosses
Grassland

Figure 2.

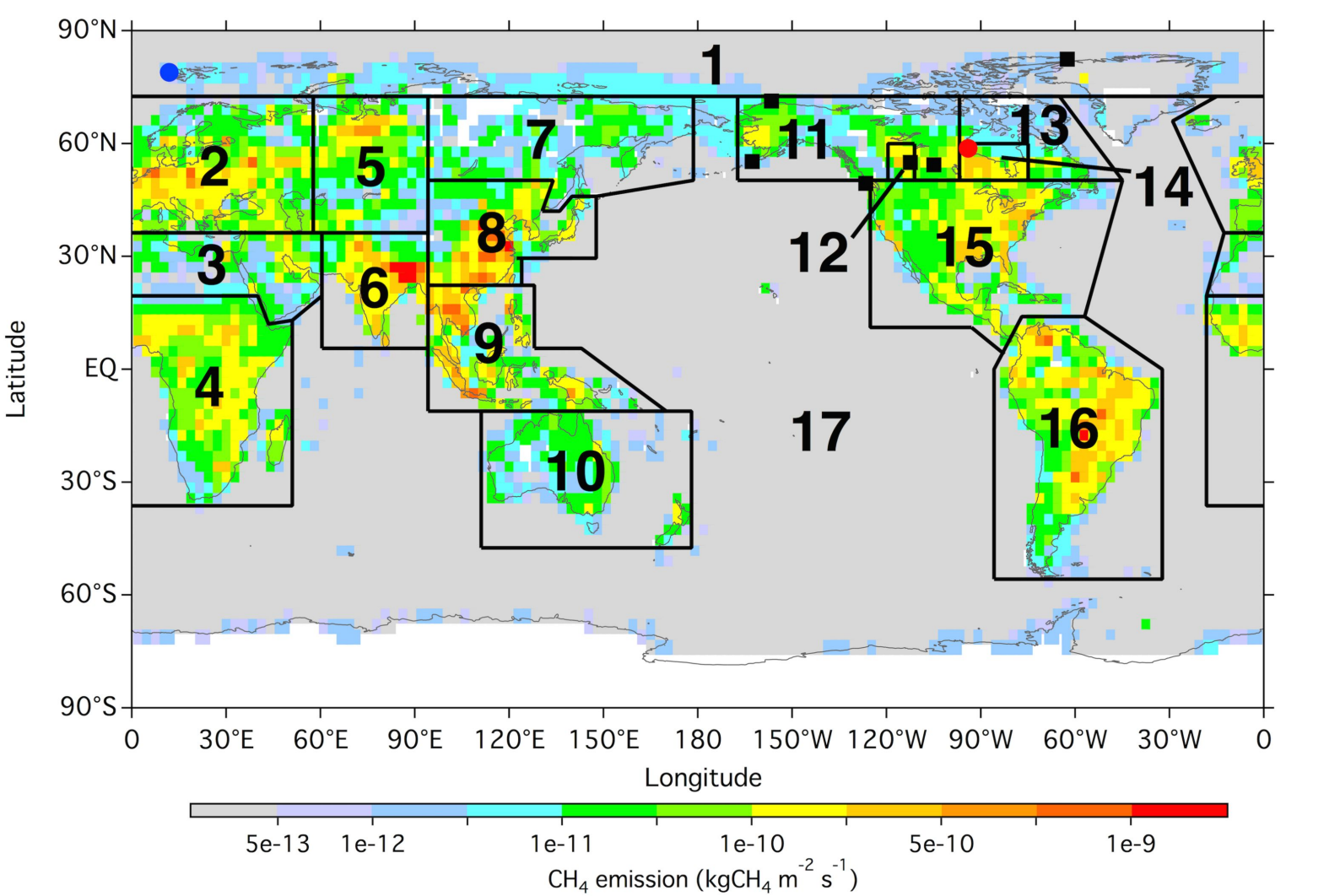
90°N
60°N
30°N
EQ
30°S
60°S
90°S
Latitude
0
30°E
60°E
90°E
120°E
150°E
180
150°W
120°W
90°W
60°W
30°W
0
Longitude
1
2
3
4
5
6
7
8
9
10
11
12
13
14
15
16
17
5e-13
1e-12
1e-11
1e-10
5e-10
1e-9
CH4 emission (kgCH4 m-2 s-1)

Figure 3.

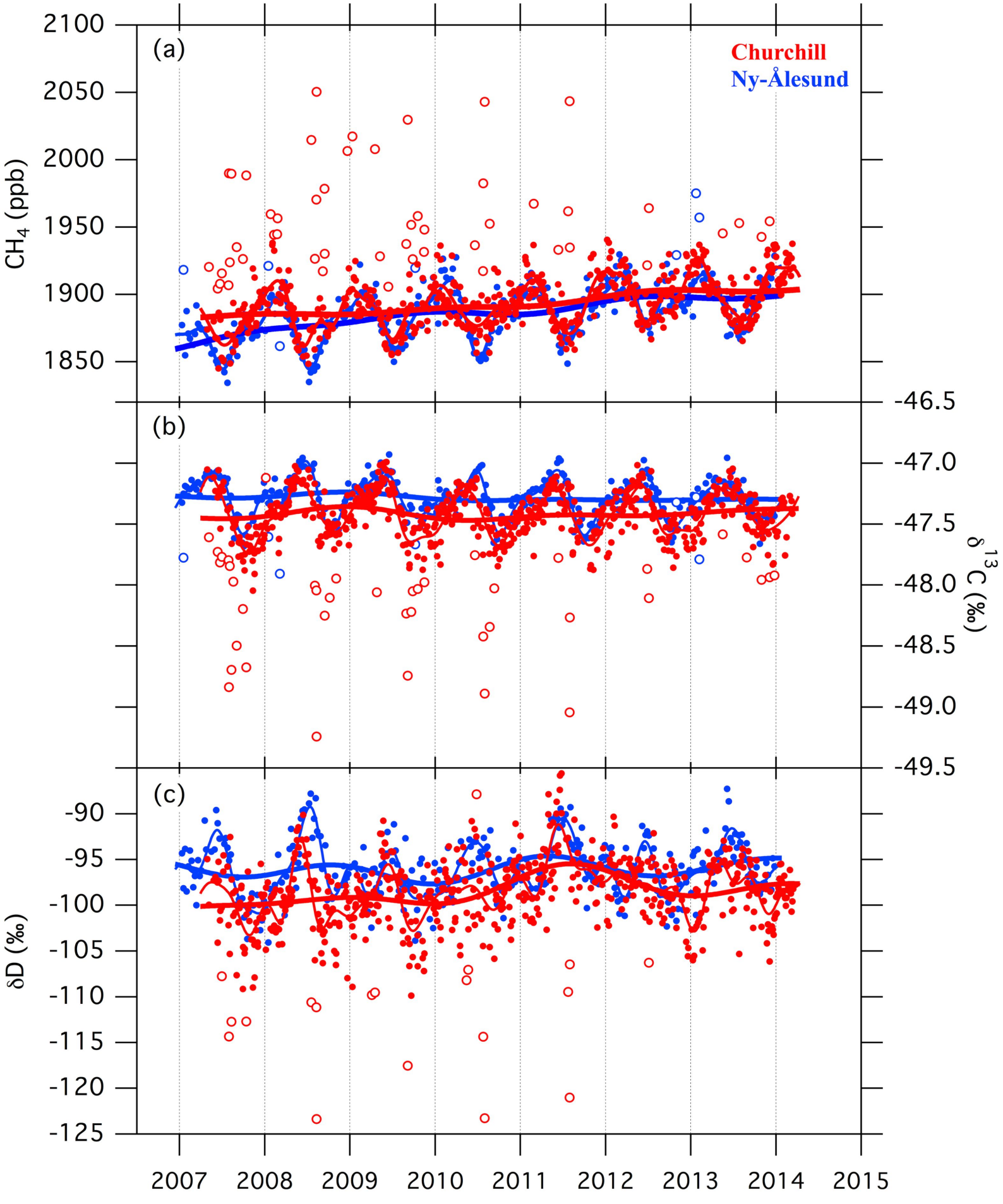
(a)
Churchill
Ny-Ålesund
CH_4 (ppb)
2100
2050
2000
1950
1900
1850
(b)
$\delta^{13}C$ (‰)
-46.5
-47.0
-47.5
-48.0
-48.5
-49.0
-49.5
(c)
δD (‰)
-90
-95
-100
-105
-110
-115
-120
-125
2007
2008
2009
2010
2011
2012
2013
2014
2015

Figure 4.

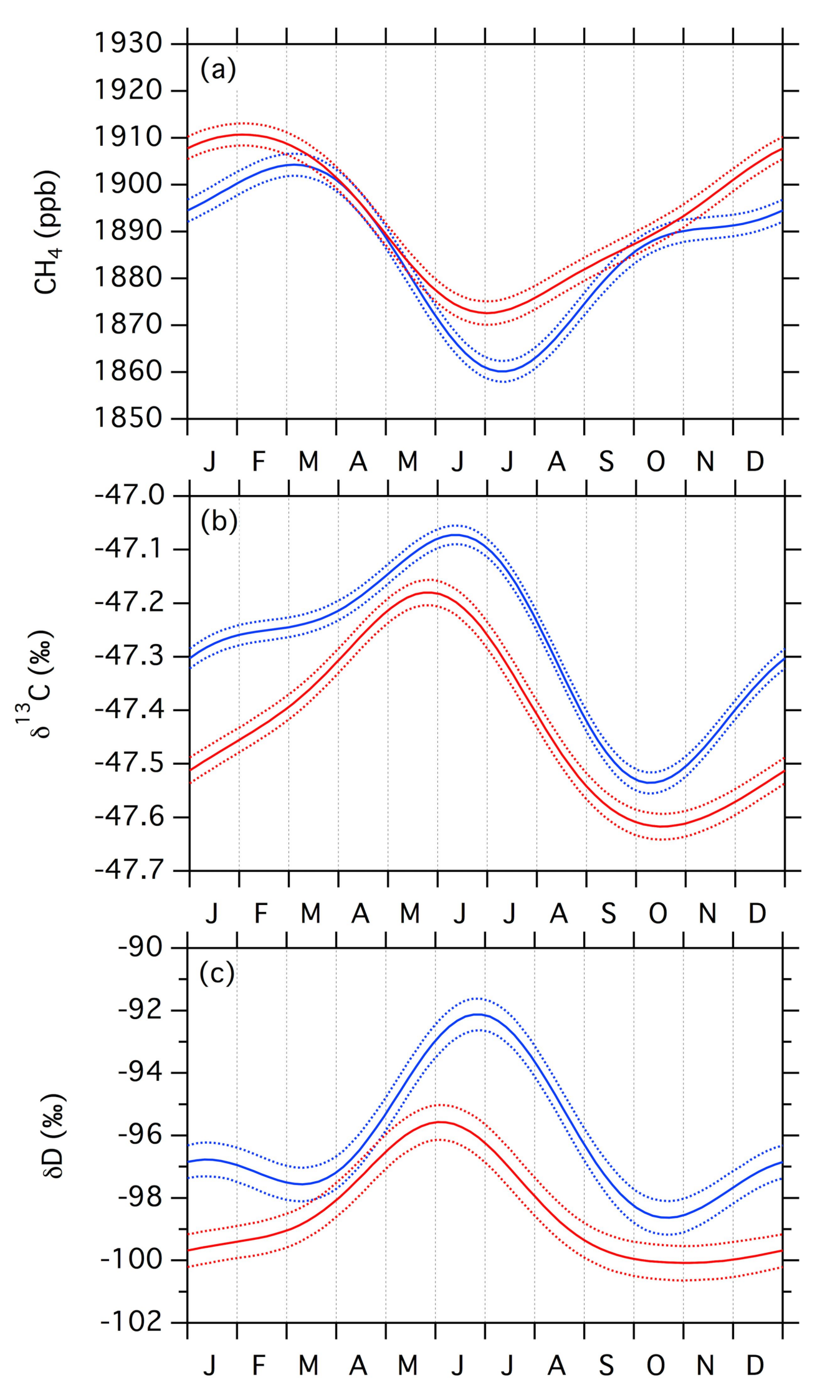
(a)
CH_4 (ppb)
1930
1920
1910
1900
1890
1880
1870
1860
1850
J F M A M J J A S O N D
(b)
$\delta^{13}C$ (‰)
-47.0
-47.1
-47.2
-47.3
-47.4
-47.5
-47.6
-47.7
J F M A M J J A S O N D
(c)
δD (‰)
-90
-92
-94
-96
-98
-100
-102
J F M A M J J A S O N D

Figure 5.

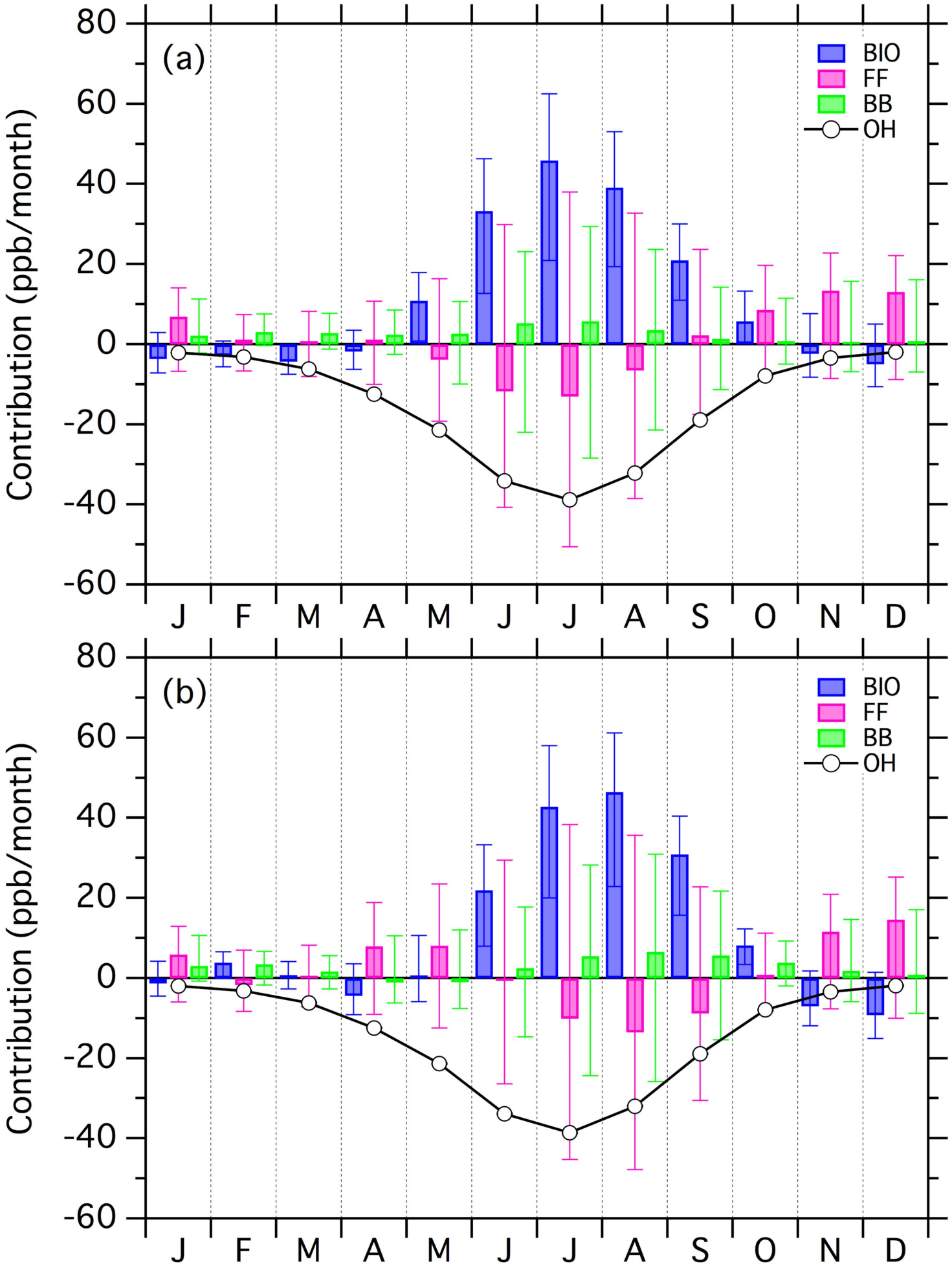
(a)
(b)
BIO
FF
BB
OH
Contribution (ppb/month)
80
60
40
20
0
-20
-40
-60
J
F
M
A
M
J
J
A
S
O
N
D

Figure 6.

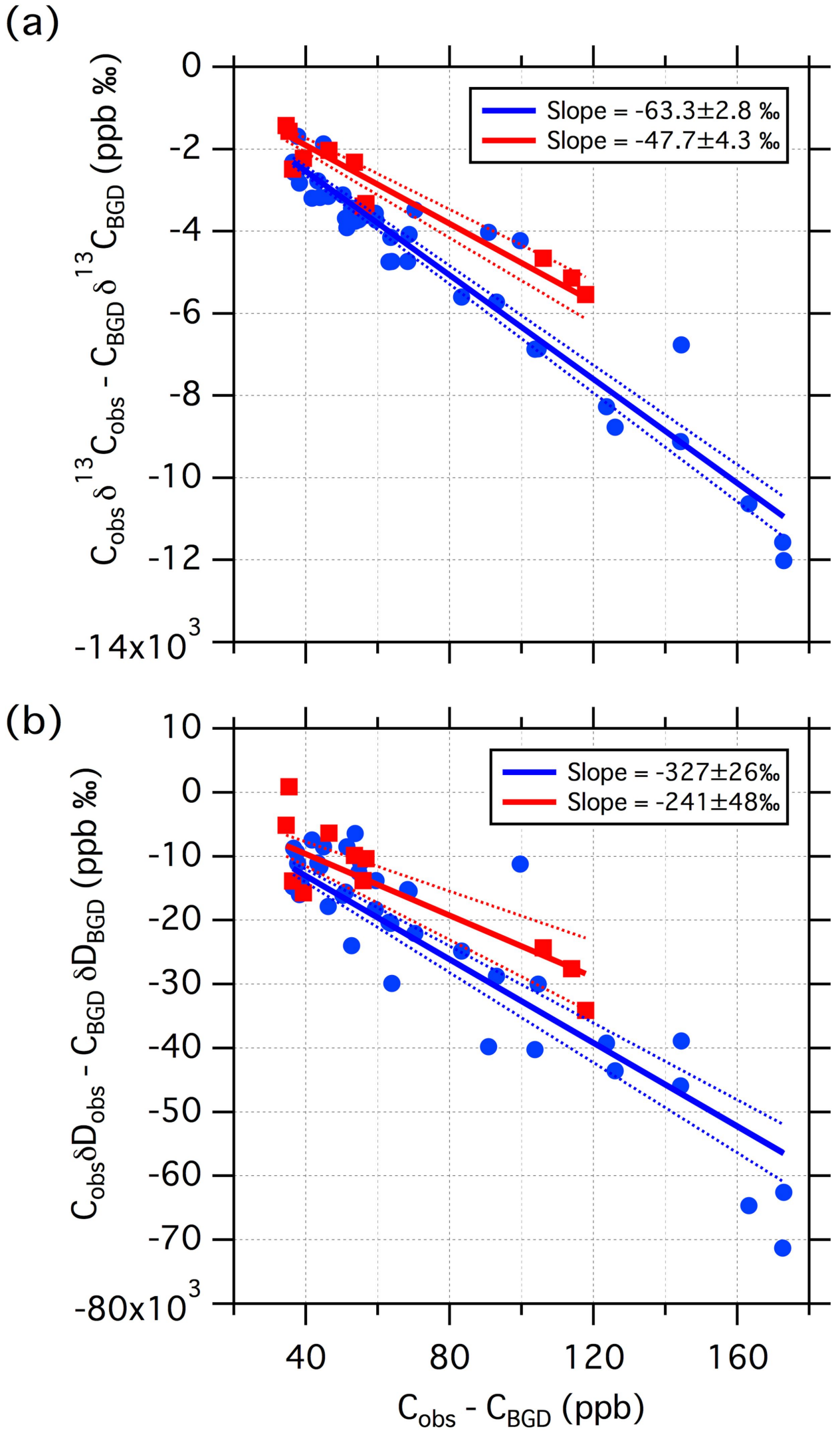
(a)
Slope = -63.3±2.8 ‰
Slope = -47.7±4.3 ‰
$C_{obs}\delta^{13}C_{obs} - C_{BGD}\delta^{13}C_{BGD}$ (ppb ‰)
0
-2
-4
-6
-8
-10
-12
$-14x10^3$
(b)
Slope = -327±26‰
Slope = -241±48‰
$C_{obs}\delta D_{obs} - C_{BGD}\delta D_{BGD}$ (ppb ‰)
10
0
-10
-20
-30
-40
-50
-60
-70
$-80x10^3$
40
80
120
160
$C_{obs} - C_{BGD}$ (ppb)

Figure 7.

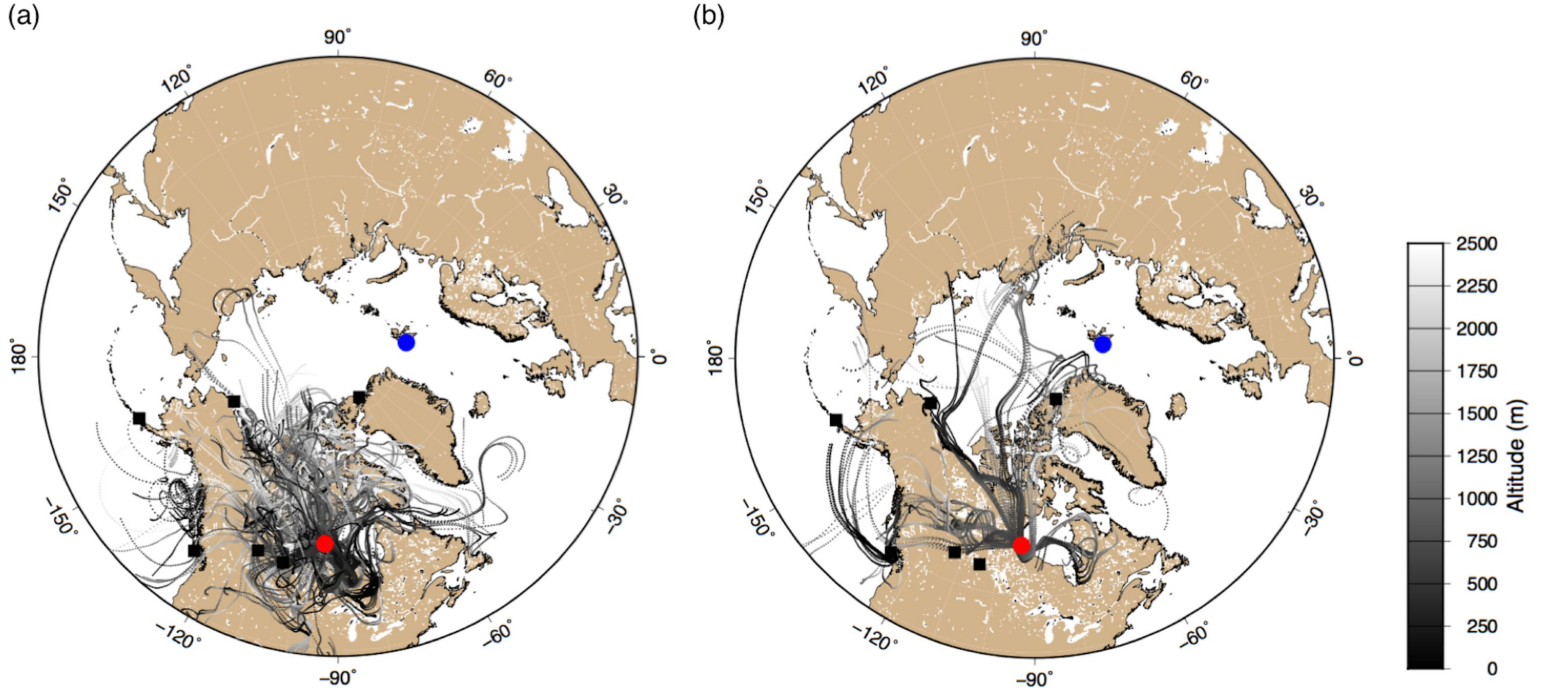
(a)
(b)
90°
120°
60°
150°
30°
180°
0°
−150°
−30°
−120°
−60°
−90°
2500
2250
2000
1750
1500
1250
1000
750
500
250
0
Altitude (m)

Figure 8.

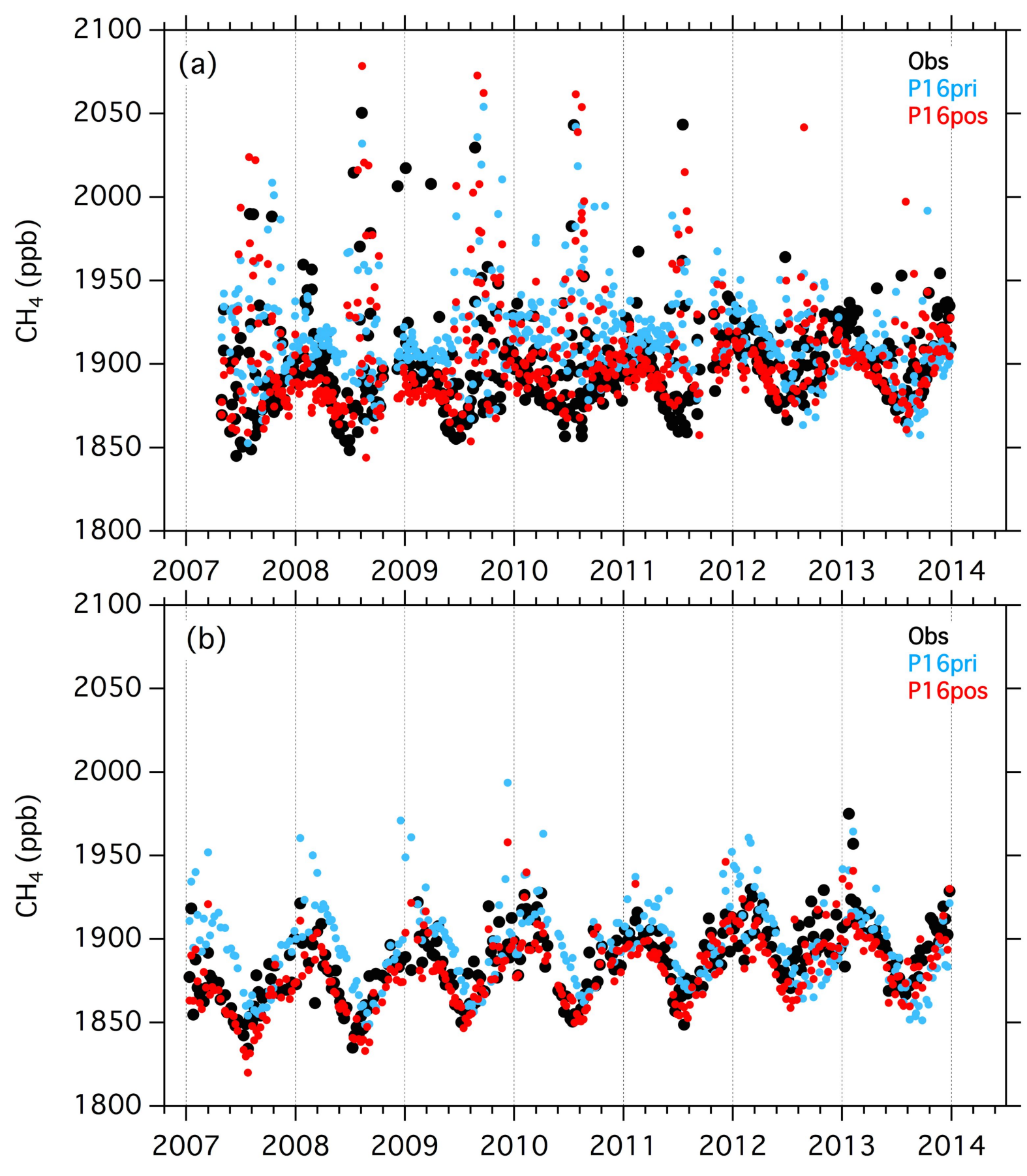
(a)
Obs
P16pri
P16pos
CH4 (ppb)
2100
2050
2000
1950
1900
1850
1800
2007
2008
2009
2010
2011
2012
2013
2014
(b)
Obs
P16pri
P16pos
CH4 (ppb)
2100
2050
2000
1950
1900
1850
1800
2007
2008
2009
2010
2011
2012
2013
2014

Figure 9.

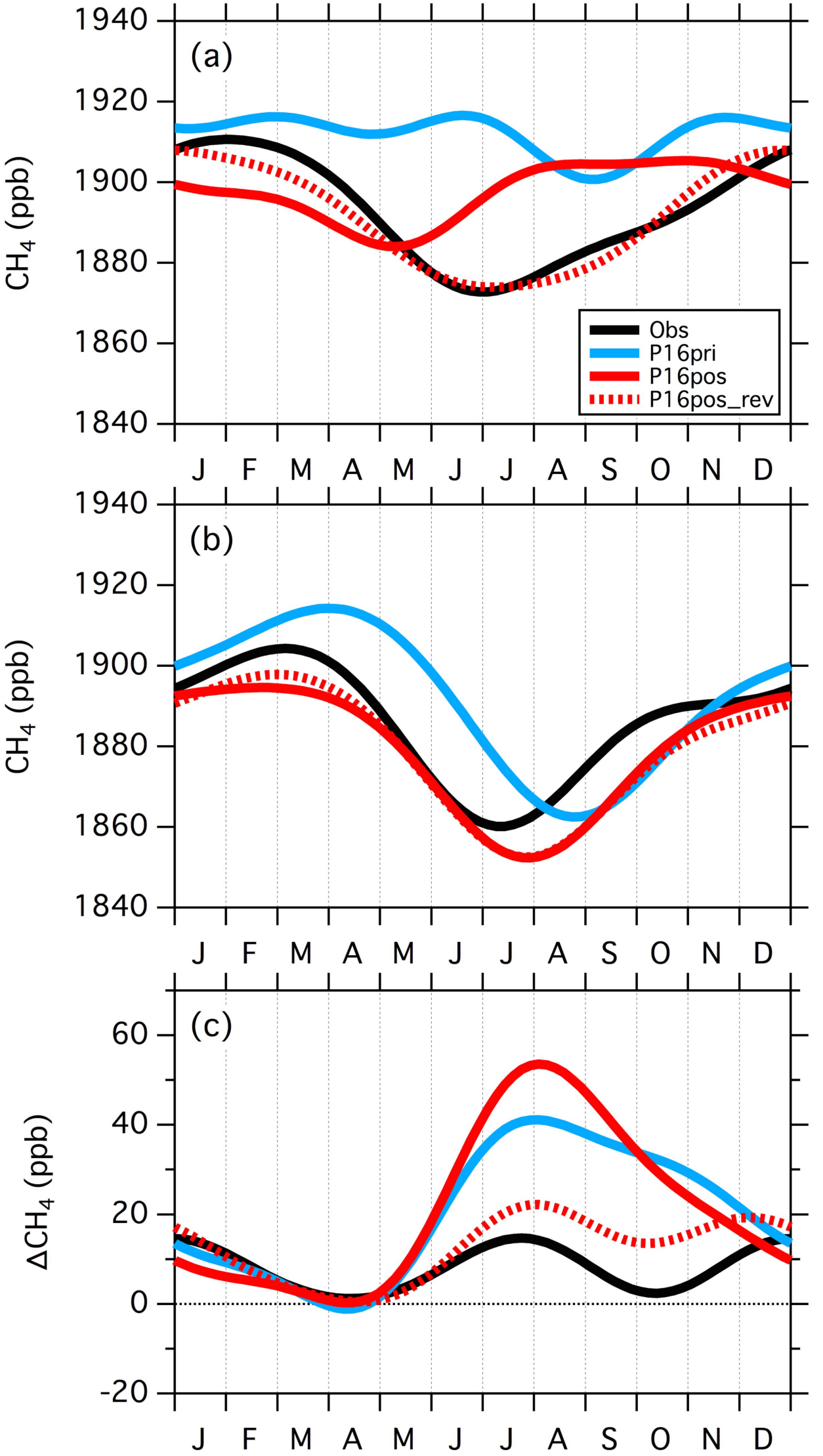
(a)
(b)
(c)
CH_4 (ppb)
ΔCH_4 (ppb)
1940
1920
1900
1880
1860
1840
60
40
20
0
-20
J F M A M J J A S O N D
Obs
P16pri
P16pos
P16pos_rev

Figure 10.

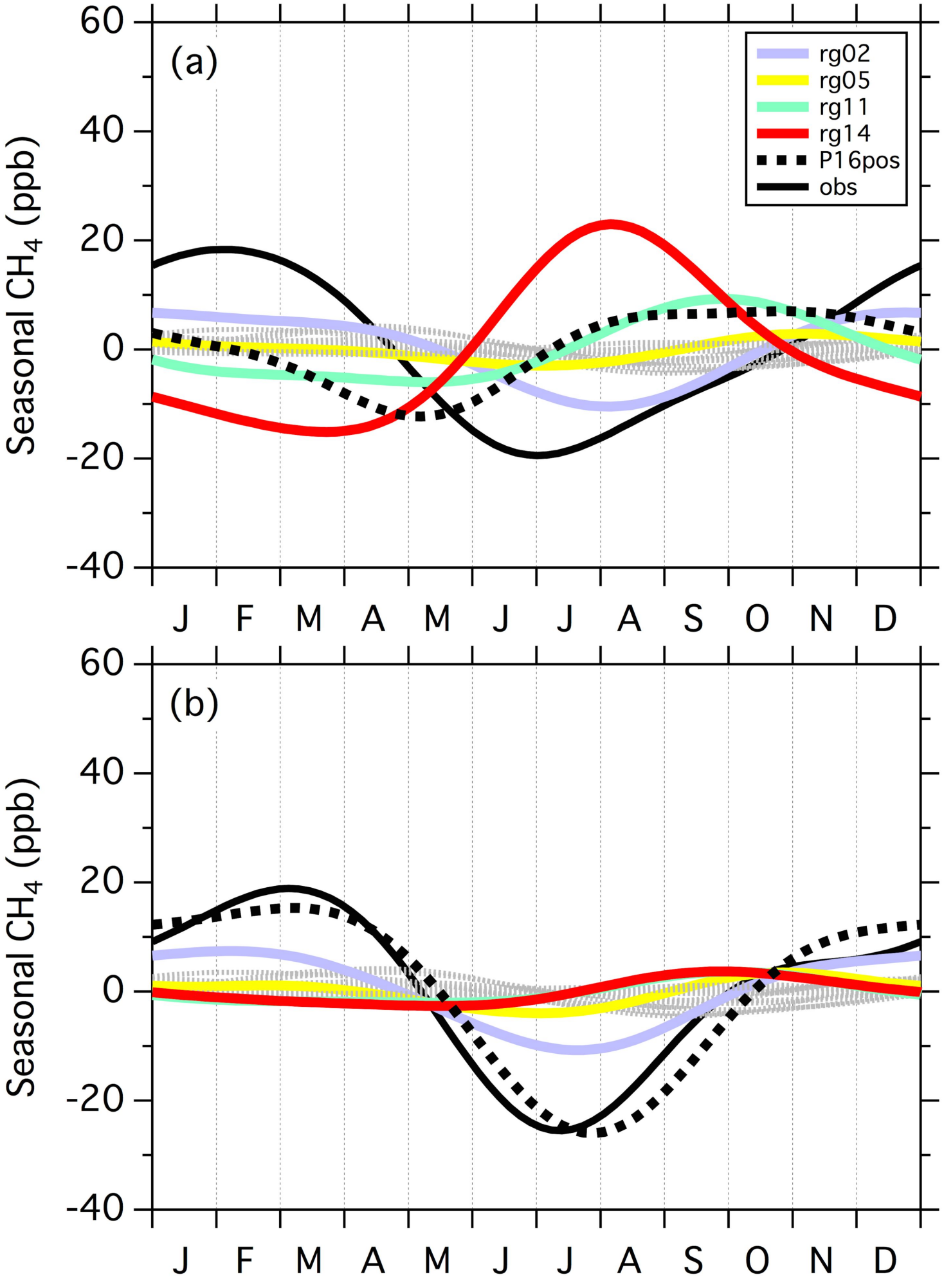
(a)
(b)
rg02
rg05
rg11
rg14
P16pos
obs
Seasonal CH_4 (ppb)
60
40
20
0
-20
-40
J
F
M
A
M
J
J
A
S
O
N
D